Contents lists available at ScienceDirect

Remote Sensing of Environment

journal homepage: www.elsevier.com/locate/rse

Land-cover change in the Caucasus Mountains since 1987 based on the topographic correction of multi-temporal Landsat composites

Johanna Buchner[a,*], He Yin[a], David Frantz[b], Tobias Kuemmerle[b], Elshad Askerov[c,d,e], Tamar Bakuradze[f], Benjamin Bleyhl[b], Nodar Elizbarashvili[g], Anna Komarova[h], Katarzyna E. Lewińska[a], Afag Rizayeva[a,i], Hovik Sayadyan[j], Bin Tan[k,l], Garegin Tepanosyan[m], Nugzar Zazanashvili[e,n], Volker C. Radeloff[a]

[a] SILVIS Lab, Department of Forest and Wildlife Ecology, University of Wisconsin-Madison, 1630 Linden Drive, Madison, WI 53706, USA
[b] Geography Department, Humboldt University Berlin, Unter den Linden 6, 10099 Berlin, Germany
[c] WWF Azerbaijan, 6th Boyuk Gala dongesi 11, Sabayıl rayon, 1001 Baku, Azerbaijan
[d] Institute of Zoology of Azerbaijan NASBlock 504, pass 1128, A. Abbaszade 13 Str., Baku, Az 1073, Azerbaijan
[e] Institute of Ecology, Ilia State University, 3/5 K. Cholokashvili Ave., 0162 Tbilisi, Georgia
[f] Geographic, GIS & RS Consulting Center, Bulachauri Street 10, 0260 Tbilisi, Georgia
[g] Department of Regional Geography and Landscape Planning, Tbilisi State University, 1 Chavchavadze Avenue, 0179 Tbilisi, Georgia
[h] Greenpeace Russia, Leningradsky prospekt, 26/1, 125040 Moscow, Russia
[i] Baku State University, Department of Bioecology, 23 Z. Khalilov st., AZ1148 Baku, Azerbaijan
[j] Forestry Department, Armenian Agricultural Academy, Teryan 74, 375009 Yerevan, Armenia
[k] NASA Goddard Space Flight Center, Greenbelt, MD 20771, USA
[l] Science Systems and Applications, Inc., Lanham, MD, USA
[m] Center for Ecological-Noosphere Studies NAS RA, GIS and Remote Sensing Department, 68 Abovyan str., Yerevan, Armenia
[n] WWF Caucasus Programme Office, 11 M. Aleksidze Street, 0193 Tbilisi, Georgia

ARTICLE INFO

ABSTRACT

Mountainous regions are changing rapidly across the world due to both land-use change and climate change. Given the importance of mountainous regions for ecosystem services and endemic biodiversity, monitoring these changes is essential. Satellite data provide a great resource to map land-cover change in mountainous regions, however mapping is especially challenging there because topographic complexity affects reflectance. The so-called 'topographic effect' has been successfully corrected for in case studies of small areas, but a comparison of large-area classifications and land-cover change analyses with and without topographic correction is missing. Here, we performed a long-term land-cover change assessment for a large mountainous region, i.e., the Caucasus Mountains with topographic correction. Our two goals were 1) to examine the effect of topographic correction on land-cover classification for a large mountainous region, and 2) to assess land-cover changes since 1987 across the Caucasus based on the full Landsat archive. Both the complex topography and the history of land-use changes, especially after the collapse of the Soviet Union in 1991, make the Caucasus Mountains an ideal study area to understand topographic effects on large-area land-cover mapping for the last three decades. First, we compared a non-topographically-corrected Landsat classification for 2015 with a classification that was topo-graphically-corrected with an enhanced C-correction for the same year and assessed the accuracy of both. Second, we derived topographically-corrected Landsat classifications for six dates to assess changes in cropland and forest from 1987 to 2015, based on class probabilities and post-classification comparisons. In regard to our first goal, topographic correction improved the overall accuracy of the classification only by 2% (from 79 to 81%), but disagreement rates were as high as 100% in mountainous regions, especially among forest types. In regard to our second goal, we found that cropland loss was the most prevalent change process since 1987. Cropland loss was particularly widespread in Georgia and Armenia until 2000, and in Azerbaijan until 2005. The North Caucasus (the Russian Federation) had more stable cropland over time, most likely due to different land reforms after the collapse of the Soviet Union, and the prevalence of flat landscapes and very fertile soils, which make cultivation easier than in the South Caucasus. Rates of forest change throughout the Caucasus Mountains were surprisingly low, with forest loss and forest gain being roughly equal. Forest loss was most likely related to both illegal logging and natural disturbance, whereas forest gain was most likely due to cropland abandonment

*Corresponding author.
E-mail address: buchner2@wisc.edu (J. Buchner).

and less grazing pressure. Our results highlight both the importance and the feasibility of topographic correction for accurate large-area land-cover classifications in steep terrain.

1. Introduction

Mountainous regions have a unique environment, harbor rich biodiversity, are high in endemism, and provide important ecosystem services such as water supply and recreation (EEA, 2010). However, mountainous regions are often subjected to land-use changes and climate changes, both of which impact mountain environments substantially. For example, forests in mountainous regions are often under threat due to illegal logging and livestock grazing (Bhatta et al., 2018; García-Ruiz et al., 1996). Mountainous areas are also often hotspots of agricultural abandonment resulting in forest expansion, particularly on steep slopes where cultivation is labor-intensive, for example, in the European Alps (Gellrich and Zimmermann, 2007; MacDonald et al., 2000). Changes in climate have contributed to increased tree mortality in some areas, but also increased growth and tree line shifts in other areas (Kulakowski et al., 2011). Further, extreme weather events such as drought can have detrimental effects on agricultural production, especially in regions where water is scarce (Lipper et al., 2014). Last but not least, land-use change and climate change often interact (Oliver and Morecroft, 2014), and to identify the causes of changes in land cover in mountainous regions, and ultimately ensure their sustainable management, it is necessary to map their spatial and temporal patterns accurately.

Land-cover changes in mountains require long-term observation with high-spatial resolution to ensure accurate mapping. With the opening of the Landsat archive (Woodcock et al., 2008; Wulder et al., 2012) the spatial and temporal coverage of satellite imagery has increased substantially, opening new opportunities for land-cover mapping such as gap-free imagery composites for large areas that overcome the challenges of limited, cloud-free data availability for large-areas (Griffiths et al., 2013; White et al., 2014). Such composites ensure that satellite image analyses are no longer restricted to scenes that are cloud-free in their entirety, and include all pixels that are not affected by clouds (Griffiths et al., 2013). Similarly, multi-seasonal imagery composites derived from Landsat imagery can capture phenological patterns among different parts of a study area. Phenology-adapted compositing algorithms dynamically adjust for spatial and temporal variations in land surface phenology due to, e.g., climate or altitude, and choose observations that matches the phenological phase of interest best (Frantz et al., 2017). Additionally, image metrics (e.g., average, standard deviation or percentiles) created during the compositing process based on all available cloud-free observations can provide valuable information for land-cover classifications (Bleyhl et al., 2017; Frantz et al., 2017; Gómez et al., 2016).

However, in mountainous regions land-cover mapping is challenging because of topographic effects (Tan et al., 2013; Vanonckelen et al., 2013). Topographic illumination effects due to shadows and steep slopes alter reflectance and thereby introduce classification errors (Vanonckelen et al., 2014). Topographic correction methods aim to remove these effects by calculating the radiance a pixel would have received and reflected without topography (Liang, 2005). Multiple topographic correction algorithms have been proposed to eliminate topographic effects. These algorithms can be categorized into three different types. First, empirical approaches only considering image-based statistical relationships that transform pixel reflectance so that the correlation between reflectance and illumination condition derived from a Digital Elevation Model (DEM) is eliminated (Tan et al., 2013). Second, physically based models model the transfer of radiance through the atmosphere to the target pixel and back (Balthazar et al., 2012). Third, semi-empirical models combine empirical and physical terms,

via the inclusion of both image-based statistics and physical formula. The C-correction is one such semi-empirical model and compares favorably to other correction methods (Riano et al., 2003; Richter et al., 2009; Sola et al., 2016). The original C-correction has been improved to a modified C-correction, which includes an additional empirically derived parameter C (Frantz, 2019; Frantz et al., 2016; Kobayashi and Sanga-Ngoie, 2008). In prior studies, topographic correction of Landsat imagery improved land-cover classification accuracy in general (Moreira and Valeriano, 2014) and of forest mapping in particular to distinguish between forest types (i.e., coniferous forest and mixed forest) (Vanonckelen et al., 2013; Yin et al., under review). Topographic correction also increased overall accuracy of forest change maps up to 34% (Tan et al., 2013). However, most studies testing topographic correction have been limited to one or two Landsat footprints (e.g., Balthazar et al., 2012; Dorren et al., 2003; Hantson and Chuvieco, 2011; Li et al., 2015; Moreira and Valeriano, 2014), and very few have analyzed large areas (Flood et al., 2013; Frantz et al., 2016; Rufin et al., 2019). A topographically corrected Sentinel-2 product is made available by ESA since May of 2019, but the USGS does not offer operational correction for the Landsat data, and there is little information how topographic correction can affect broad-scale land-cover classification accuracy. In the era of Analysis Ready Data (ARD), an automatic approach for atmospheric and topographic correction of satellite imagery covering large areas is of growing importance though. Our aim was thus to test the feasibility and effectiveness of topographic correction for large-area mapping, and we selected the Caucasus Mountains as our study area. The Caucasus Mountains with their high elevation range and complex land-cover patterns are an ideal study area to assess the value of topographic correction for land-cover mapping of large areas.

The Caucasus underwent major institutional and political changes after the collapse of the Soviet Union in 1991 when the transition from a planned economy to a market-oriented economy altered institutions and triggered land reforms (Hartvigsen, 2014). The countries of the Caucasus implemented different land reforms regarding land ownership, affecting primarily agriculture and forests (Hartvigsen, 2013). The Russian Federation mostly distributed agricultural land through land shares to individuals, who often leased their acquired land shares back to large corporate farms, ultimately limiting the fragmentation of the land ownership. In Georgia, Armenia, and Azerbaijan, collective farms were privatized, and parcels were distributed to new owners resulting in a high fragmentation of both ownership and land use with an average parcel size of < 2.8 ha (Giovarelli and Bledsoe, 2001; Hartvigsen, 2014, 2013; Spoor, 2004; Terra Institute, 2005). Forest was also state-owned during Soviet times and highly protected under the Soviet forest code since the 1950s (FAO, 2019). Public ownership and management of forests remained in the Caucasus region after the collapse (FAO, 2019). However, enforcement of environmental regulations varies, and there have been several armed conflicts in the Caucasus region raising the question of how land cover, particularly cropland and forest, has changed since the collapse.

Our overall goals were thus 1) to compare large-area Landsat classification accuracy for non-topographically-corrected versus imagery that was topographically-corrected with an enhanced C-correction, and 2) to map gains and losses of croplands and forests, the timing of these changes, and differences in these change trajectories among countries, across the Caucasus Mountains from 1987 to 2015. These two goals were mutually dependent. Our first, technical goal required to evaluate a land-cover classification in a large mountainous region, and our second goal, mapping land-cover changes in a mountainous region with steep terrain required topographic correction to obtain accurate results.

2. Methods

2.1. Study area

Our study area encompassed Georgia, Armenia and Azerbaijan in the south (South Caucasus) and parts of the Russian Federation in the north (North Caucasus), with a total area of 455,000 km^2 and included two major mountain ranges: the Greater Caucasus Mountain Range and the Lesser Caucasus Mountain Chain (Fig. 1) (Zazanashvili et al., 2012). The mountains in the Greater Caucasus range from 500 to 3000 m a.s.l. in the west but are lower eastwards towards the Caspian Sea (Volodicheva, 2002). The so called Side or Parallel range contains the tallest mountains peaking at 5642 m a.s.l. at Mount Elbrus in the western part. Precipitation exceeds 2000 mm per year in the coastal area close to the Black Sea (Zazanashvili et al., 1999). The majority of the mountains in the Lesser Caucasus range from 2000 to 2800 m a.s.l. in

the west and 2500 to-3300 m a.s.l. in the south-east with the highest point of 4090 m a.s.l. at Mount Aragats in Armenia (Volodicheva, 2002). Similar to the Greater Caucasus, the Lesser Caucasus has wet climate in its western part, but is more continental and dry in the eastern and south-eastern parts (Zazanashvili et al., 1999).

The Caucasus region contains seven major vegetation zones: deserts and semi-deserts, steppes, sparse arid woodlands, forests, subalpine woodlands, subalpine meadows, and alpine meadows (Gulisashvili, 1964; Volodicheva, 2002). Semi-deserts occur in southern Armenia and Nikhichevan, Azerbaijan, and along the coast of the Caspian Sea. Steppes occur in both the North Caucasus and South Caucasus, but have been heavily modified by humans and are largely replaced by agriculture. In the Russian part, secondary steppe occurs on the highlands of Stavropol and on lower elevation slopes of the Greater Caucasus. In the south, steppes occur on plains and upper mountain ranges of Armenia. The transitional zone between semi-desert and forests is
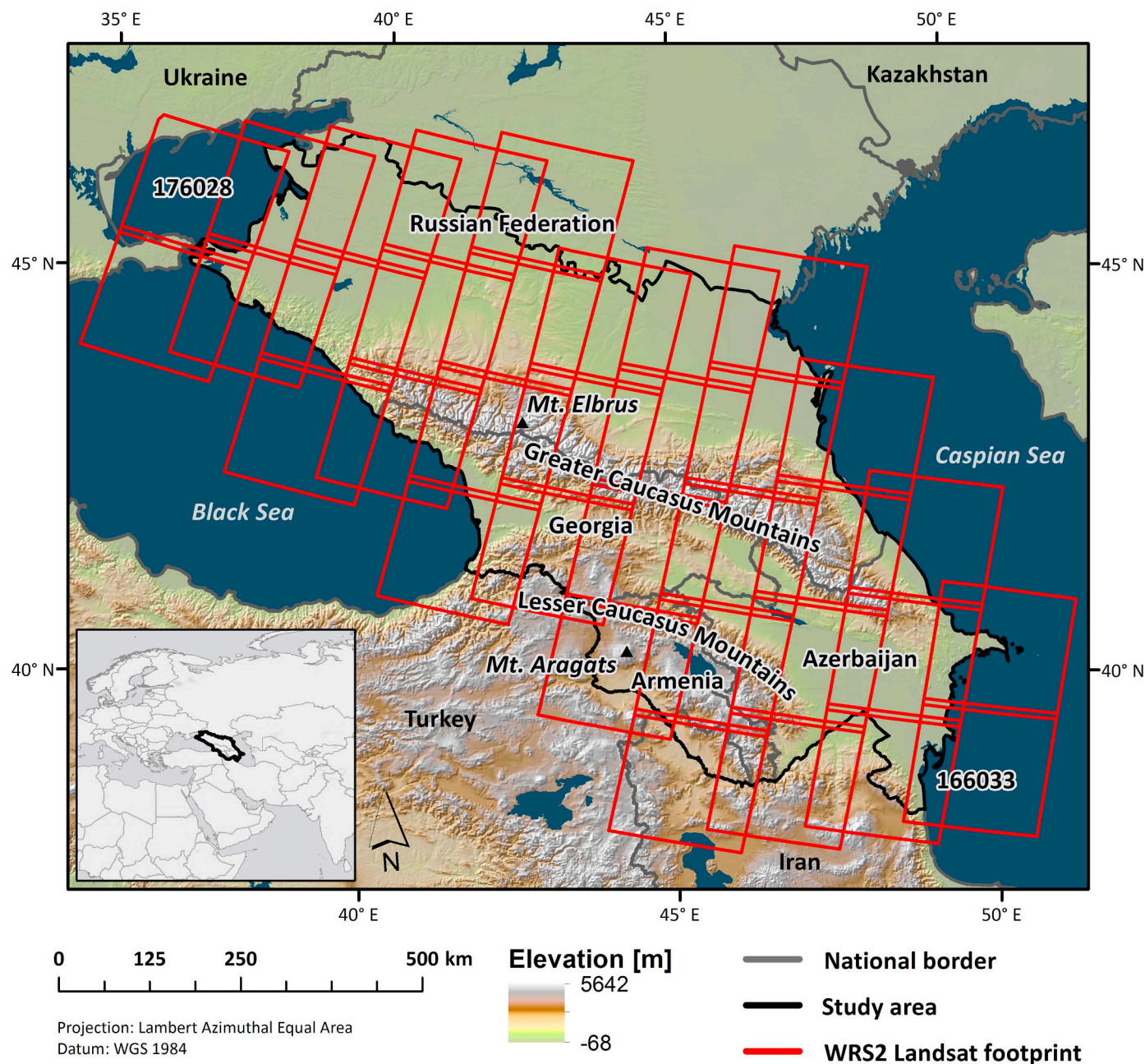

Fig. 1. Overview of the 35 WRS2 Landsat footprints covering the Caucasus study area between the Black Sea and the Caspian Sea, including parts of the Russian Federation in the north, and Georgia, Armenia and Azerbaijan in the south.

typically covered by sparse arid woodland. Natural formations of this vegetation type remain in eastern Georgia, Azerbaijan, and Karabakh. Forests span across the entire Caucasus and occur from sea level up to 2700 m a.s.l. Forests are often dominated by one or two species and species'-rich forests are fairly rare. Mixed and coniferous forests, including spruce (*Picea orientalis*), fir (*Abies nordmanniana*), and pine (*Pinus* spp.), are typical for the western part of the Caucasus at higher altitudes, whereas deciduous forests, including monodominant beech (*Fagus orientalis*), oak (*Quercus* spp.), oak and hornbeam (*Qercus-Carpinus caucasica*), and chestnut and hornbeam (*Castanea sativa-Carpinus caucasica*), are typical at lower elevations and towards the east. Forests transition into subalpine woodlands in higher altitude, but both being threatened by wood cutting and grazing. Subalpine woodlands are succeeded by subalpine meadows and alpine meadows between 2300 and 3700 m (Gulisashvili, 1964; Volodicheva, 2002).

The countries of the South Caucasus, i.e., Georgia, Armenia, and Azerbaijan are relatively small with a population of 3.7 million, 2.9 million, and 9.6 million in 2015, respectively (World Bank Data, 2019a), especially when compared to their northern neighbor, the Russian Federation. Russia's North Caucasian Federal District, which covers parts of our study area, had a population of 9.4 million in 2010 (Rosstat, 2010). Both the North Caucasus and the countries of the South Caucasus are highly agrarian and have a high rural population (Holland, 2016; Lerman, 2009; O'Loughlin et al., 2007). The agricultural sector is important for employment, economic growth, poverty reduction, and food security (Welton et al., 2013). Agricultural employment rates in Georgia, Armenia, and Azerbaijan were 44%, 35%, and 36% in 2015 and agriculture provided 7%, 18%, and 6% of the country's GDP respectively in 2010 (World Bank Data, 2019b). Agriculture is predominantly carried out by individual households and is often a mix of crop and fruit production and small-scale animal husbandry, with specific products such as wine, nuts, cognac, or sugar concentrated in individual countries (Ahouissoussi et al., 2014; Welton et al., 2013). The republics of the North Caucasus were famous for their potato production during Soviet times, but the economy of the region was weaker compared to other republics in Russia after the collapse. Although increasing social polarization occurred in the North Caucasus, agriculture remains important for rural livelihoods and some republics experienced rising consumer demands, which created an increase of agricultural products such as wheat, corn, sunflower, and fruits (O'Loughlin et al., 2007; Rada et al., 2017).

2.2. Image processing

We processed 12,651 L1T Landsat TM/ETM+/OLI images from the USGS archive acquired between 1985 and 2016, i.e., all available images with < 70% cloud cover for 35 WRS-2 footprints covering the Caucasus Mountains (Fig. 1). We processed the imagery with the Framework for Operational Radiometric Correction for Environmental monitoring (FORCE) software (version 1.1 beta, available at http://force.feut.de) (Frantz, 2019; Frantz et al., 2016). FORCE is based on the radiative transfer theory and includes both atmospheric and topographic correction, as well as a correction for adjacency effects to estimate Bottom-of-Atmosphere (BOA) reflectance. Topographic correction is included in the form of an enhanced C-correction in FORCE (Frantz et al., 2016). Please refer to Appendix A at the end of the paper for a detailed description of FORCE and the implemented topographic correction.

All images were projected to Lambert Azimuthal Equal Area (Datum: WGS 1984, latitude of origin: 42.5, central meridian: 43.5) with a spatial resolution of 30 m and were organized as data cubes with a tile size of 30 × 30 km.

In order to generate a gap-free dataset of clear-sky observations, we used FORCE to calculate pixel-based composites for six target years (1987, 1995, 2000, 2005, 2010, 2015, including +/− 1 year for 1995, because we expected most changes during the transition period, and

+/− 2 years for the others ones). We analyzed multi-year time steps, because image availability from 1987 to 1995 was too limited for annual analyses (SI Fig. A1).

We embedded land surface phenology in the compositing process to account for phenological differences related to both climatic variability and topographic complexity (Frantz et al., 2017). We calculated land surface phenology by pooling all available observations across all years to one annual set, because the number of cloud-free Landsat pixels was too limited to derive annual phenology, especially from 1985 to 1995. We used the Spline analysis of Time Series (SpliTS) algorithm to calculate land surface phenology (Mader, 2012). SpliTS derives phenological parameters (e.g., beginning and end of the growing season) by fitting polynomial splines to a time series of enhanced vegetation index (EVI) values and extracts parameters thereof. The pixel-based land surface phenology dynamically adjusts the target date for each pixel in an image composite (Frantz et al., 2017). We choose the following key vegetation stages such as start of season (SOS), which is the timing of year when vegetation growth begins, peak of season (POS), which is timing of maximum vegetation growth, and end of season (EOS), which is the timing when senescence occurs, for our analysis. We defined the extracted phenological parameters, i.e., SOS, POS, and EOS as the anchor sequence for the three image composites (SI Fig. A2). We calculated land surface phenology only for one set of imagery, the uncorrected images, because our motivation for calculating this phenology was to account for the strong climatic gradient from east to west, and the elevation gradient. Furthermore, we needed to ensure that the target dates for our composites were the same for both the topographically-corrected and non-topographically corrected datasets. We determined the suitability of each observation for each seasonal composite based on several scores, i.e., acquisition day, acquisition year, distance to clouds or cloud shadows, potential contamination with haze, spectral correlation, and off-nadir view angle. A detailed description of the derivation of these scores is provided in Frantz et al. (2017). The total score S_T was computed as the weighted linear combination of the scores following Frantz et al. (2017):

$$S_T = \frac{\sum WS}{\sum W} \tag{1}$$

where S denotes the phenology-adapted suitability of the acquisition day (S_D) and year (S_Y), the probability of cloudiness (S_C), the potential contamination with haze (S_H), the spectral correlation (S_R) and the view zenith angle (S_V), and W denotes the weight for each score. The highest total score defined the best observation which in turn was used for the seasonal composite (Frantz et al., 2017). In addition we calculated spectral-temporal metrics for each season to take advantage of all clear observations and to represent the variability of the land surface during the compositing period (target year +/− 2 years) (Frantz et al., 2017; Griffiths et al., 2013) (SI Fig. A3, SI Table A1, SI Table A2). We calculated average, 25% quantile, 50% quantile, 75% quantile, range, standard deviation, and the number of observations for each spectral band for each of the three seasons.

In order to quantify the effect of topographic correction on land-cover classification, we calculated one set of Landsat imagery and seasonal composites for 2015 that were topographically-corrected and a second set of Landsat imagery and composites that were not topographically-corrected (detailed workflow SI Fig. A4).

2.3. Land-cover classification with and without topographic correction

In our land-cover classifications we separated 10 land-cover classes namely coniferous forest, mixed forest, deciduous forest, barren, rangeland, cropland, built-up, wetlands, water, and snow and ice. In order to obtain training samples for all classes, we digitized polygons in areas that were both homogenous and stable over time according to high-resolution imagery in Google Earth, field visits, and the Climate Engine

web app (Huntington et al., 2017) and assured that training samples were located across the study area to capture the heterogeneity of the landscape. Forest types were identified based on their phenology in fall and winter imagery and mixed forest was defined as woody vegetation with neither coniferous nor deciduous tree species covering > 70% of the canopy. Cropland was identified based on the shape of the cultivated fields, evidence of plowing, and the homogenous green-up cover during one year. Areas with sparse vegetation, shrubs, and grassland were defined as rangeland. Barren was defined as high altitude areas in rocky terrain and areas with no vegetation cover (SI Fig. A5). We randomly collected 2000 training pixels within the polygons of each class with a minimum distance of 30 m, and combined these with training samples that were available for two footprints in our study area from previous studies that followed the same land-cover classification scheme and mapped land-cover classes such as stable cropland, as well as different forest types and grassland (Yin et al., 2018b, Yin et al., under review). Our final set of training samples consisted of 9.7% coniferous forest, 9.1% mixed forest, 10.8% deciduous forest, 10% barren, 10.1% rangeland, 11.7% cropland, 9.5% built-up, 9.5% wetlands, 10% water, and 9.7% snow and ice. As input for our 2015 non-topographically and topographically-corrected classifications, we used the three seasonal Landsat composites plus the following spectral-temporal metrics, i.e., average, 25% quantile, 50% quantile, 75% quantile, range, standard deviation, and number of observations, calculated for each season (Bleyhl et al., 2017; Griffiths et al., 2013; Yin et al., 2017). As our classifier, we used the R package ′C5.0′ (Kuhn and Quinlan, 2018) for all classifications. ′C5.0′ is a decision tree classifier that consists of a collection of tree-structured classifiers and can accommodate missing values (Friedl et al., 2002; Quinlan, 1986). By using ′C5.0′ we were able to keep pixels with missing values in the seasonal composites by using values from the spectral-temporal metrics layers for the classification instead. We applied adaptive boosting with 100 trials. Ultimately, we calculated the per-pixel class probability based on the percentage of tree votes for each given class.

Initial results showed strong confusion between built-up, rangeland, and barren land, with built-up having a high commission error. In order to better separate the built-up class from other classes, we used class probability and a calibration approach (Yin et al., 2018a). Specifically, we sampled 200 validation points with < 50% probability and 200 validation points with > 50% probability of the built-up class for each time step, and labeled them based on high-resolution imagery in Google Earth. Based on these 400 validation points we calculated user's and producer's accuracy for different probability thresholds for the build-up class (i.e., probability > 50%, > 60%, > 70%, > 80%, and > 90%). The threshold that yielded the most balanced user's and producer's accuracy was selected for mapping the built-up class (SI Fig. A6) (Yin et al., 2018a). Every built-up pixel that was below the probability threshold was assigned to the second-highest ranked class. Furthermore, based on visual interpretation, we label pixels above 2000 m a.s.l that were classified as 'built-up' as 'rangeland'. In a final step, we applied a minimum mapping unit of 8 connected pixels and assigned smaller areas to the nearest neighboring class. We applied the same post-classification rules to both the non-topographically and the topographically-corrected classification.

In order to understand in which parts of our study area the topographic correction made the biggest difference, we summarized the disagreement between the non-topographically-corrected and the topographically-corrected classifications in a 300-m grid. Furthermore, we summarized the disagreement results based on the cosine correction term A_{CC} for the annual classification as follows:

$$A_{CC} = \left(\frac{\cos \Theta_{SSOS}}{\cos i_{SOS}} + \frac{\cos \Theta_{SPOS}}{\cos i_{POS}} + \frac{\cos \Theta_{SEOS}}{\cos i_{EOS}} \right)/3 \qquad (2)$$

where Θ_S denotes the solar zenith angle and i denotes the solar incidence angle, both for the different seasons. Values above 1 indicate

shaded areas, and values below 1 indicate brightened areas. Cos i is defined a-s in eq. (6) in Appendix A.

2.4. Land-cover change assessment for 1987, 1995, 2000, 2005, 2010, and 2015

Based on our results for 2015 (see section 3.1) we analyzed cropland and forest changes after 1987 using only topographically-corrected composites because they yielded higher classification accuracy. Data processing for all the remaining target years (1987, 1995, 2000, 2005, and 2010) followed the steps outlined for year 2015 in section 2.3. For our cropland change assessment, we retained two classes, 'cropland' and 'non-cropland'. For the forest change assessment, we aggregated coniferous, mixed, and deciduous forest to 'forest' and the remaining classes to 'non-forest'. We applied a post-classification comparison based on the classification maps for the six time steps. We did not classify change classes directly, because changes were generally rare making it infeasible to collect sufficient training samples for each of the 20 changes classes among the six time steps for both cropland and forest. In a final step, we applied a 3×3 window majority filter for both the cropland change map and the forest change map to reduce noise.

To compare cropland loss and gain, and forest loss and gain among different countries, regions and time steps, we calculated relative net changes (RNC) following Kuemmerle et al. (2009) as:

$$RNC = \left(\frac{L_{i+1}}{L_i} - 1 \right) 100$$
$$i = \{1987, 1995, 2000, 2005, 2010\} \qquad (3)$$

where L denotes the land class (either cropland or forest in km^2), and i denotes the time step.

2.5. Accuracy assessment

We validated both the non-topographically-corrected and the topographically-corrected classification map for 2015 by calculating overall accuracy, user's and producer's accuracy (Congalton, 1991), and the F1-score. The F1-score was calculated following Powers (2011) as:

$$F1 = \frac{2 \, UA \, PA}{UA + PA} \qquad (4)$$

where UA denotes user's accuracy, and PA producer's accuracy. The F1-score ranges from 0 to 1, being 1 when both UA and PA are 1, and being 0 if either UA or PA is 0. Greater differences between UA and PA result in a lower F1-score (Powers, 2011).

We selected a disproportionate stratified sampling approach for our validation samples to account for small classes (Olofsson et al., 2014; Stehman et al., 2003). We generated a total of 1553 validation samples (SI Table A3), randomly sampled within each class of the topographically-corrected map and corrected the resulting confusion matrix by the area proportions of each class (Griffiths et al., 2014; Olofsson et al., 2014). For the accuracy assessment of the non-topographically-corrected map we used the same validation samples. Because the strata of the topographically-corrected map differed spatially from the non-topographically-corrected map, we took the inclusion probability of the validation samples into account to derive unbiased estimators (Stehman, 2014; Yin et al., 2018b). All samples for the accuracy assessment of the topographically-corrected classification were visually interpreted and labeled by two independent interpreters using high-resolution images in Google Earth and time series of the normalized difference vegetation index (NDVI), the bare soil index (BSI), and tasseled cap wetness calculated from the original Landsat imagery for 2015 in Google Earth Engine (Gorelick et al., 2017; Yin et al., 2020a).

For the validation of our change detection maps, we selected new samples, and calculated overall, user's and producer's accuracies (Congalton, 1991). For both the cropland and the forest change map we

aggregated some of the change classes, and kept single classes only when one consistent change and no deviations in any year occurred (example 1: 1987-'95: cropland and 2000-'15: non-cropland; example 2: 1987-'00: non-cropland and 2005-'15: cropland). Classes with a deviation in any year were aggregated to a 'transitional' class (e.g., 1987-'95: cropland, 1995-'00: non-cropland, and 2005-'15: cropland). We applied disproportional random sampling for both the cropland and the forest change map. We randomly selected 50 validation samples for each cropland and each forest change class. Because the transitional cropland class was much larger than the transitional forest class, we

selected 150 validation samples for the former and 50 validation samples for the latter. Furthermore, we selected 150 validation samples each for the stable non-cropland class, stable non-forest class, stable cropland class, and stable forest class. In total, we generated 950 validation samples for the cropland change map and 850 validation samples for the forest change map (Olofsson et al., 2014). Samples for the change detection assessment were visually interpreted and labeled by only one interpreter, who was very familiar with the study region and the prevailing land-cover changes, using high-resolution images in Google Earth, and plotting NDVI, BSI, and tasseled cap wetness times
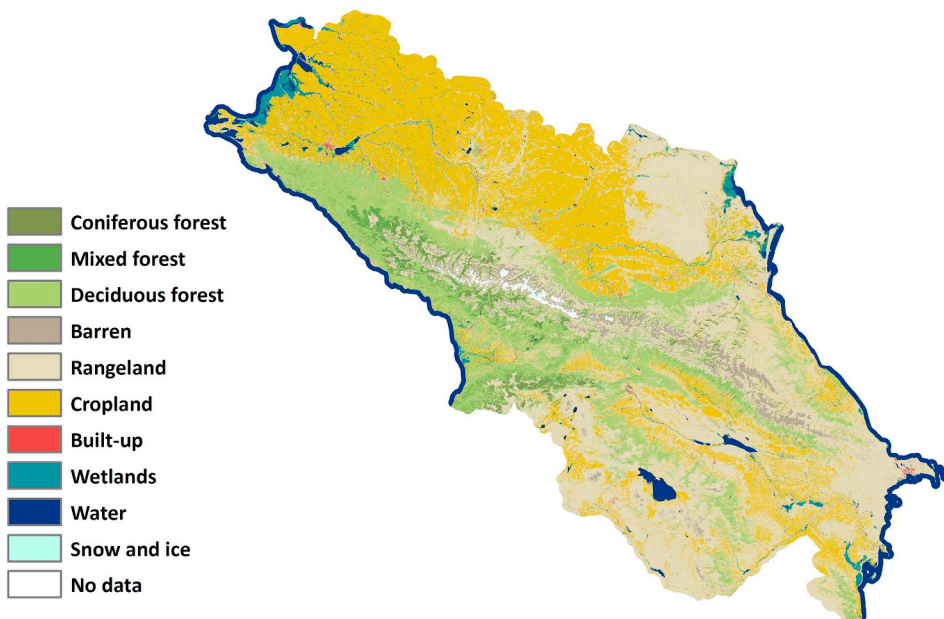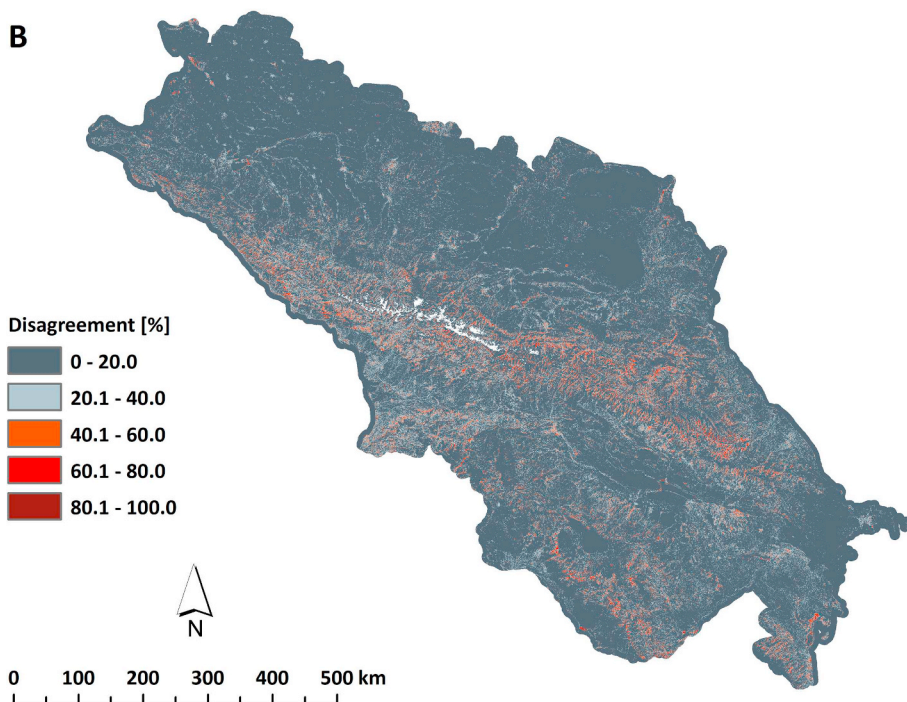

Fig. 2. (A) Topographically-corrected land-cover classification for 2015 and (B) disagreement in percent between non-topographically-corrected and topographically-corrected classification maps summarized in a 300-m grid for visualization and analysis purposes.

series based on 1985–2016 Landsat imagery in Google Earth Engine to detect changes (Gorelick et al., 2017; Yin et al., 2020a). Lastly, we calculated the error matrix with estimated proportions of area for both the cropland change map and the forest change map.

3. Results

3.1. Effects of topographic correction on land-cover mapping

Applying topographic correction improved the overall accuracy of the 2015 classifications from 79.4 ± 0.9% to 81.2 ± 1.8% (SI Table A4, SI Table A5). The error adjusted area estimates for our topographically-corrected classes were the largest for rangeland (175,787 km^2 ± 14,904 km^2), followed by cropland (142,669 km^2 11,522 km^2), deciduous forest (72,669 km^2 ± 9593 km^2), water (21,066 km^2 ± 5210 km^2), barren (11,408 km^2 ± 3069 km^2), wetlands (11,062 km^2 ± 2308 km^2), mixed forest (10,455 km^2 ± 3662 km^2), coniferous forest 7685 km^2 ± 1670 km^2), built-up (1466 km^2 ± 2552km^2), and ice and snowsnow and ice (564 km^2 ± 135 km^2) (Fig. 2, SI Fig. A7).

User's accuracy for the non-topographically-corrected map was highest for deciduous forest (87%) and lowest for mixed forest (23%) (Fig. 3). User's accuracy for the topographically-corrected map was generally higher and highest for rangeland (89%) and lowest for mixed forest (36%). The topographically-corrected classification had higher user's accuracies for all three forest types (coniferous forest (65%), mixed forest (36%), deciduous forest (88%)) compared to the non-topographically-corrected classification (coniferous forest (48%), mixed forest (23%), deciduous forest (87%)). Producers' accuracy was always higher for the topographically-corrected classification map, except for two classes (mixed forest and rangeland). Confidence intervals for producer's accuracy were always smaller for the topographically-corrected classification, except mixed forest (Fig. 3).

The F1-score of the topographically-corrected map outperformed the non-topographically-corrected map for all but two classes (barren and snow and ice) (Fig. 3). Topographic correction improved the F1-score of the coniferous forest class by 0.15 change points, deciduous forest by 0.05, mixed forest by 0.04, and rangeland, and cropland by 0.01 change points.

We found that barren, coniferous forest, mixed forest, and deciduous forest occurred on steeper slopes (on average 26.57°, 25.97°, 23.15°, and 17.15° respectively). Rangeland occurred on slopes with an
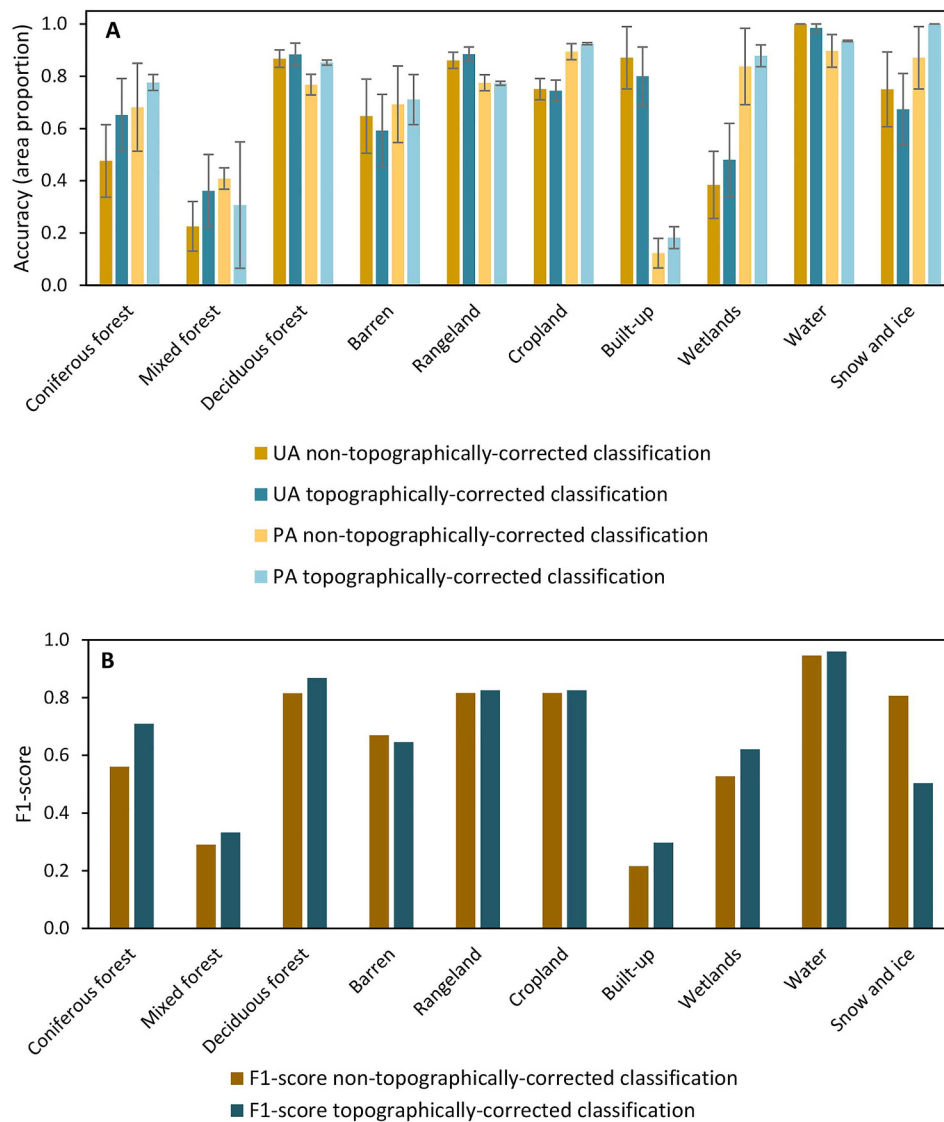

Fig. 3. (A) Area adjusted user's accuracies (UA) and producer's accuracies (PA) of non-topographically-corrected and topographically-corrected classification. Error bars indicate the 95% confidence intervals. (B) F1-score based on user's and producer's accuracy of non-topographically-corrected and topographically-corrected classification.

average of 10.35° and cropland, built-up, wetlands, and water occurred in flat terrain with an average slope smaller than 3° (SI Table A6). We found the highest disagreement in class assignments between the non-topographically-corrected and the topographically-corrected maps along the crests of both the Greater and the Lesser Caucasus Mountain ranges (Fig. 2). We observed the lowest agreement for the mixed forest class (SI Fig. A8). When summarizing the disagreement by A_{CC}, disagreement was generally highest in extreme conditions, i.e., with very high A_{CC} (Fig. 4). In areas that were moderately shaded or moderately brightened the disagreement rates were slightly higher for shaded areas than for bright areas. Disagreement rates were very low for highly brightend areas, however the percentage of cells, where that was the case, was less than 0.05% of the study region. In almost flat areas where the solar zenith angle Θ_S and the incidence angle i were roughly the same, disagreement rates were lowest (7%) (Fig. 4). A good expample for this are the flat lands of the Northern Caucasus.

3.2. Cropland change

The overall cropland area decreased in all four countries when using 1987 as the baseline (Fig. 5, Fig. 6). The North Caucasus had the least amount of cropland loss, i.e., only 6% in 2000 compared to 1987. Georgia had biggest cropland loss in 2005 (-28%) and 2015 (-31%). Armenia had its highest cropland loss in 2000 (-17%), followed by an immediate increase in 2005. Armenia was the only country where cropland increased by 2% in 2010 compared to 1987. Azerbaijan went through the greatest cropland loss from 1987 to 2005 (-30%), with an increase in 2010 before again decreasing in 2015 (Fig. 6). Throughout the study region cropland loss was mainly due to the conversion of cropland to rangeland and only occasionally due to the conversion to forest. Cropland gain was mostly due to the conversion of rangeland to cropland (SI Fig. A9).

The North Caucasus had the largest extent of stable cropland (Fig. 7), 39% of the total land area was continuously in cultivation from 1987 to 2015 there, and only 8% of what was cropland in 1987 was abandoned in a later year. In contrast, in Georgia, Armenia, and Azerbaijan, only 7%, 9%, and 10% of the total land area was continuously cultivated until 2015, and 10%, 10% and 15% of cropland in 1987 was abandoned in each country, respectively (Fig. 7).

Aggregating cropland changes by administrative units (see SI Fig. A10 for names of administrative units) revealed the substantial spatial variation in land-cover change trends (Fig. 8). From 1987 to 1995 cropland decreased in all countries but Armenia, where a 6% increase was observed in its southern regions. Until 2000, Samtskeh-Javakheti and Shida Kartli in Georgia, as well as Shirak in Armenia showed a decrease in cropland. At the same time, parts of the North Caucasus, Kakheti in Georgia, and several regions in Azerbaijan had a slight increase in cropland. Between 2000 and 2005 cropland decreased in the eastern regions of the North Caucasus, Georgia and in two regions of Azerbaijan, namely Aran and Lankaran with a decrease of 14.9% and 7.4%, respectively. In Armenia, we found hardly any decrease in cropland between 2000 and 2005. In Azerbaijan, Aran and Lankaran had the highest increases of 13.3% and 6.6%, respectively, from 2005 to 2010, the time period during which most areas showed cropland gains. From 2010 to 2015 we observed a slight decrease in all regions in the North Caucasus and Georgia, as well as a decrease of 7.2% in Lori, Armenia. In Azerbaijan we found an increase in most regions, except Lankaran with a decrease of 7.4% (Fig. 8).

3.3. Forest change

We found far less forest changes than cropland changes (Fig. 9). Overall, forests increased during our study period (Fig. 10). Most forest gains occurred along forest edges and on abandoned cropland and were due to the conversion of barren, rangeland, and cropland to forest (Fig. 9, SI Fig. A9). Forest loss was scattered throughout the study region and mostly due to the conversion of forest to rangeland or

cropland (SI Fig. A9).

Forest area increased in the North Caucasus (6%), Armenia (8%), and Georgia (6%) from 1987 to 2015, and only Azerbaijan experienced a decrease of forest compared to 1987 (-4%) (Fig. 10). The highest forest loss rates of 6% occurred in Azerbaijan between 2000 and 2005 (Fig. 10).

We found the highest forest loss rates in earlier years and less forest loss in later years. The highest forest loss rates from 1987 to 1995 were in mountain regions in the North Caucasus, in two regions in Georgia and in the northern part of Azerbaijan (Fig. 11). During that time, Kalbajar-Lachin in Azerbaijan and Racha-Lechkhumi-Kvemo Svaneti in Georgia had the highest forest gain of 4.7% and 4.2%, respectively. From 1995 to 2000 more regions experienced forest loss than forest gain, with the highest forest loss rates occurring in two regions in Georgia, concomitant to the highest forest gain in Georgia. Between 2000 and 2005, forest loss was again more widespread than forest gain, although forest losses in the northern part of the Caucasus were minor, whereas the southern part of the Caucasus showed higher forest losses, especially in Azerbaijan. The highest forest gain occurred in Georgia (Imereti, 2.6%) and Armenia. From 2005 to 2010 forests mostly increased in Georgia, with a forest gain up to 6% in Guria. Lankaran in Azerbaijan had the highest forest loss (2.7%) for this time period. From 2010 to 2015, only one region in Georgia showed a decrease in forest higher than 2%, all other areas were more or less stable ($< 1.9\%$ change) or experienced forest gain (Fig. 11).

3.4. Change accuracy assessment

Our cropland change map had an overall accuracy of 75.7 $\pm$ 2.6%, but with high variation among classes (Table 1). We observed highest user's and producer's accuracies of 97% and 78%, respectively, for non-cropland, and 71% and 88%, respectively, for stable cropland. Cropland change classes obtained much lower accuracies ranging from 8% to 43% for user's accuracy, and from 9% to 68% for producer's accuracy. Confusion occurred mainly between the non-cropland and stable cropland classes, and change classes often showed confusion with the previous or following time step, i.e., the change was mapped correctly but its timing was not (Table 1).

The overall accuracy for the forest change map was 90.2 $\pm$ 2.7%, and similar to the cropland change map with high variation among classes (Table 2). We found highest user's and producer's accuracies of 95% and 97%, respectively, for non-forest, and 95% and 83%,
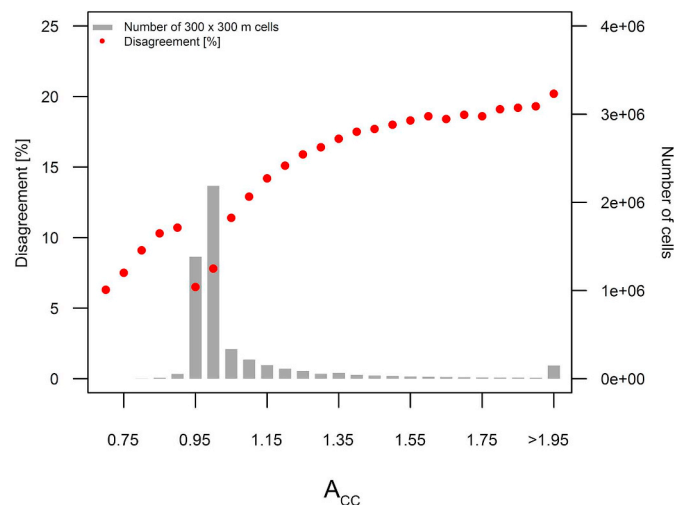

Fig. 4. Mean disagreement in percent between the non-topographically-corrected and the topographically-corrected classification in a 300-m grid based on the mean annual values of A_{CC} for 2015. Please note that bin sizes on the extreme ends differ ($0.75 < A_{CC} \leq 0.80$, $A_{CC} > 1.95$).
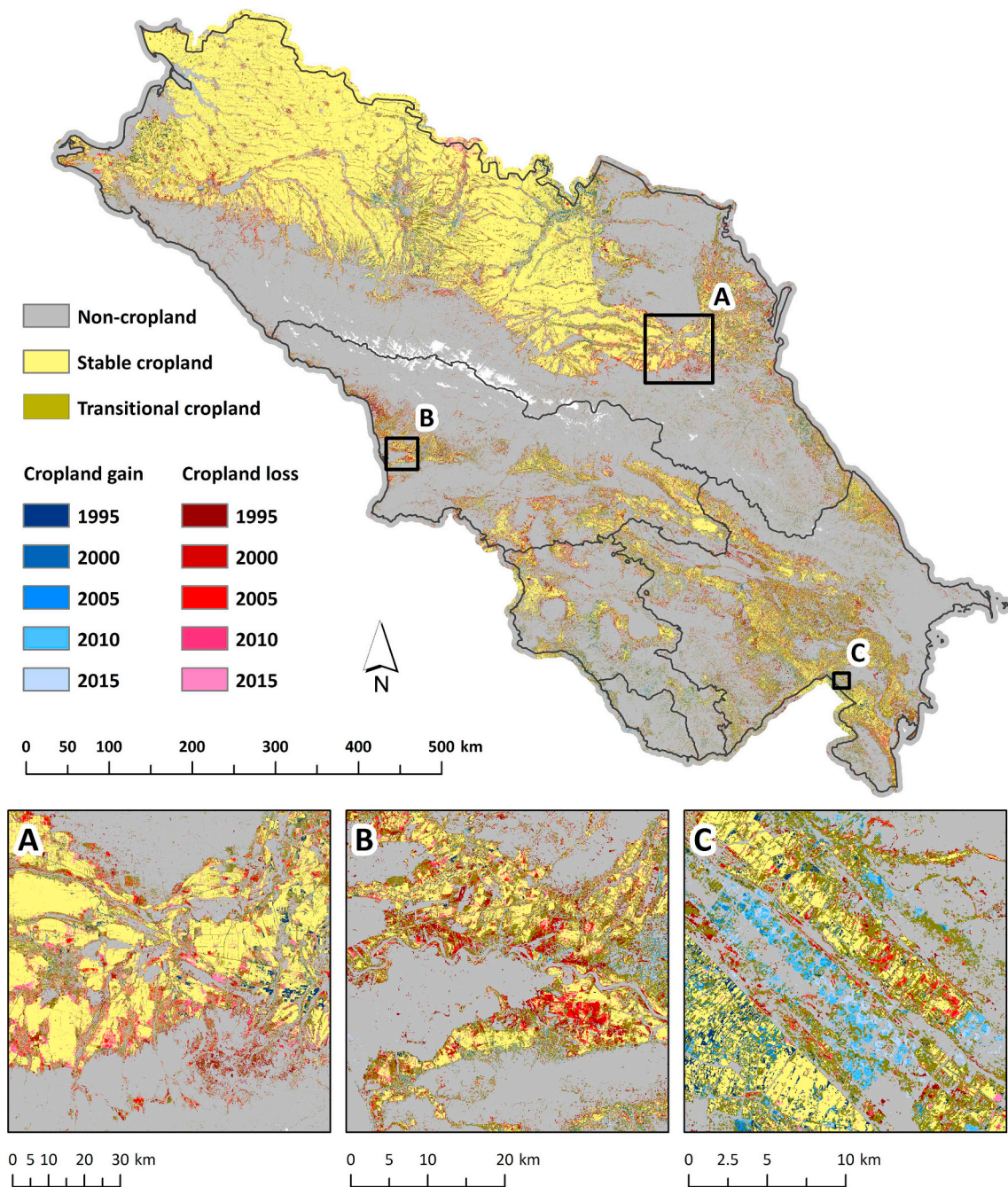
Fig. 5. Cropland gain and loss in the Caucasus region from 1987 to 2015. The transitional cropland class contains pixels that alternated between cropland gain and loss. Zoom-ins show (A) cropland loss in Chechnya (Russian Federation), (B) cropland loss in parts of Guria and Samegrelo-Zemo Svaneti (Georgia), and (C) cropland gain in Aran (Azerbaijan).

respectively, for stable forest. Our forest gain classes had lower producer's accuracies from 5% to 30%, and higher user's accuracies from 22% to 36%. The forest loss classes had higher producer's accuracies from 14% to 78%, but lower user's accuracies from 4% to 24%. Forest change classes, similar to cropland, often showed confusion with the previous or the following time step (Table 2).

4. Discussion

4.1. Effects of topographic correction on land-cover mapping

Land cover in mountainous regions is notoriously difficult to map with satellite images, because high variation in illumination conditions introduces errors in land-cover classifications. Here we show that

topographic correction for large-area and long-term analyses is feasible and can improve classifications considerably. Our results are in line with previous studies for small study areas that showed that topographic correction improves the separation of forest types (Pimple et al., 2017; Vanonckelen et al., 2013), and these results make sense given that forests are often found in steep terrain where topographic correction has the largest effect. Topographic correction also enhanced the separation of forests from other land-cover classes, such as rangeland. By applying topographic correction, we were able to improve our large-area land-cover classifications, and hence our broad-scale land-cover change assessment.

The overall accuracy of the topographically-corrected classification map improved by only 2% compared to uncorrected imagery. The reason why that number was relatively low was that the large northern
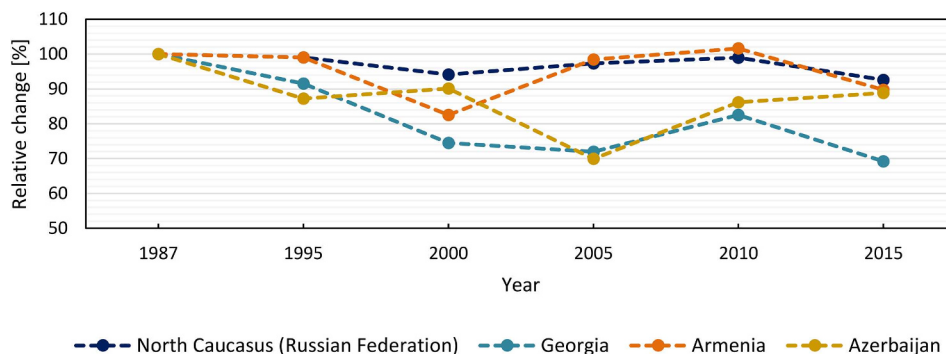
Fig. 6. Relative cropland change for six time steps with 1987 as baseline for the North Caucasus (Russian Federation), Georgia, Armenia and Azerbaijan. Note that the y-axis starts at 50%.
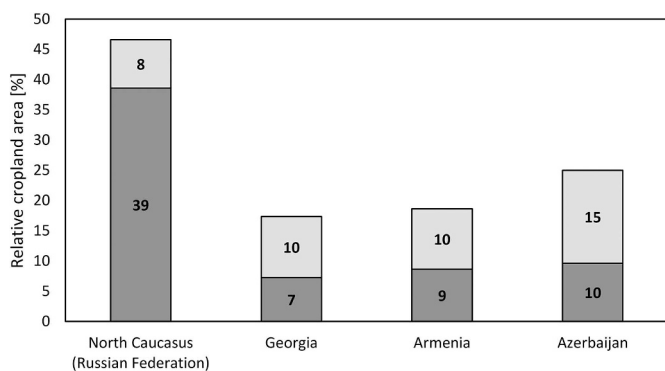

Fig. 7. Percentage of stable active cropland from 1987 to 2015 (dark grey) and of cropland in 1987 that was subsequently abandoned (light grey).

part of our study area has little topography and that is where mostly cropland and rangeland occur. Topographically-corrected imagery improved the classification especially in areas with extreme illumination conditions. In areas with steep topography, differences between the classification of topographically-corrected and uncorrected imagery were substantial, similar to what has been found previously (Vanonckelen et al., 2013; Yin et al., under review) and especially the accuracies for forest classes were higher when topographic correction was applied (Huang et al., 2008). Only two of our land-cover classes, barren and snow and ice, had a slightly higher F1-score for the non-topographically corrected classification. In a previous study of topographic correction methods for different land-cover classes (Sola et al., 2016), the intraclass interquartile range (IQR) reduction was best for the rock class, suggesting that this class is very homogenous and therefore its reflective behavior more controlled. In our case, barren
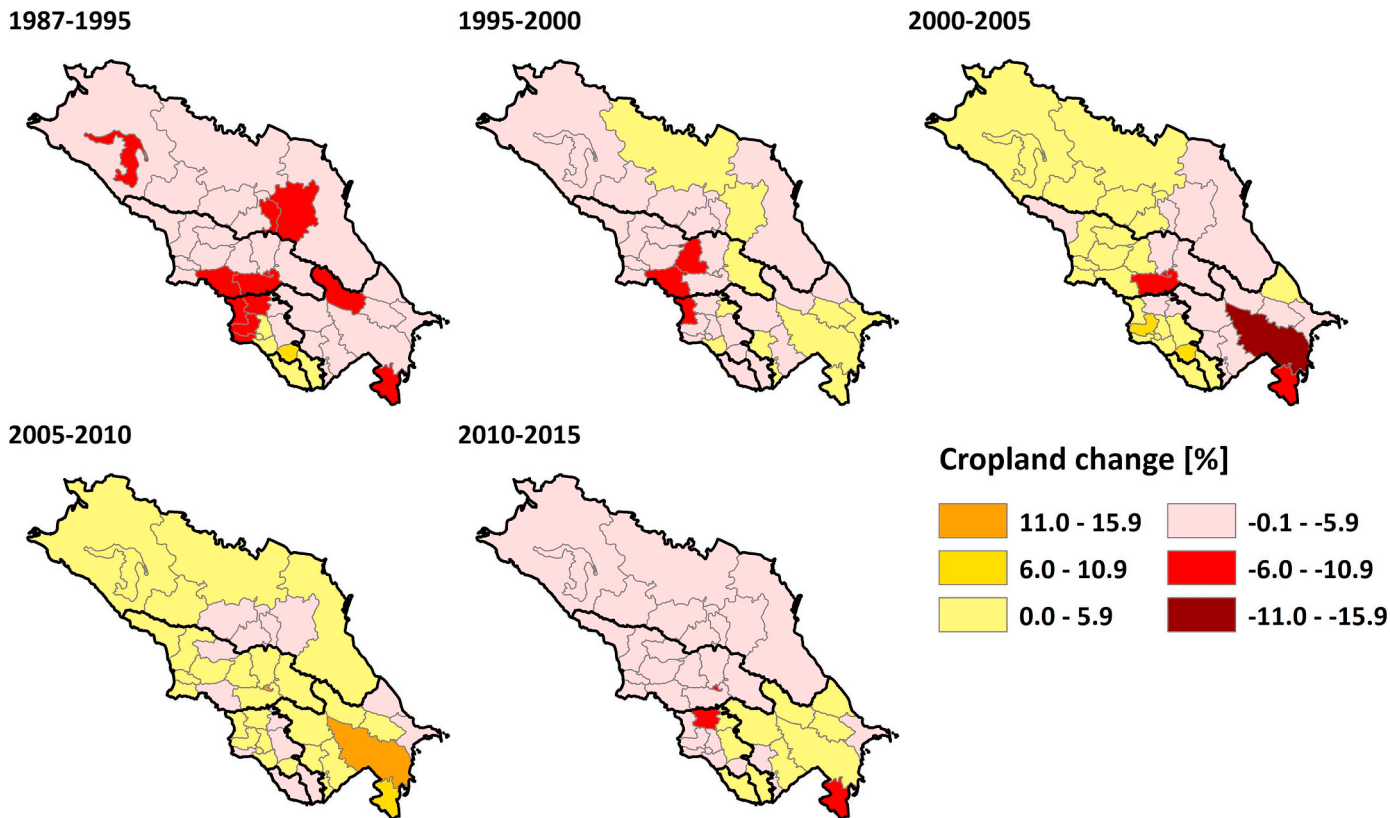

Fig. 8. Cropland change aggregated for administrative units of the North Caucasus (Russian Federation), Georgia, Armenia and Azerbaijan. Please refer to supplemental information Fig. A10 for names of administrative units.
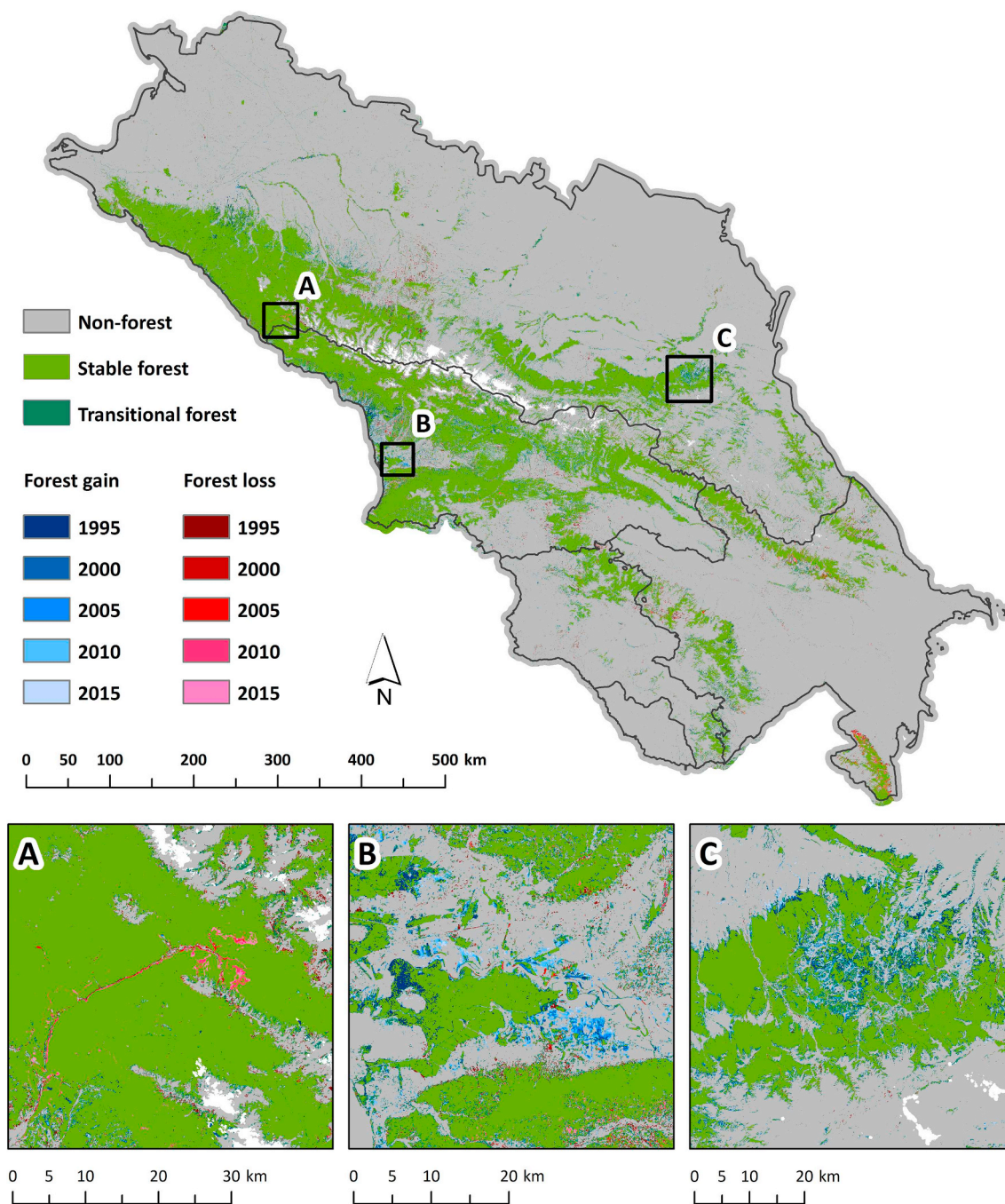
Fig. 9. Forest gain and loss in the Caucasus region from 1987 to 2015. The transitional forest class contains pixels that alternated between forest gain and loss. Zoom-ins show (A) forest loss in Sochi (Russian Federation), (B) forest gain in Guria and Samegrelo-Zemo Svaneti (Georgia), and (C) forest gain in Chechnya (Russian Federation).

and snow and ice were not homogenous, but rather often a mix of rock and ice that occurred in heavily jointed terrain with cast-shadows and very low illumination conditions. It is likely that a low availability of same-class pixels in the local pixel neighborhood resulted in an unreliable estimate of the regression parameters for the C-factor. Thus, the topographic correction potentially produced less accurate corrections. Indications for this can be derived from SI Fig. A11, where a lower number of same-class pixels is apparent for snow-covered areas – although a lower number of available pixels does not result in lower R^2 for all land-cover classes. A second potential reason for the slightly higher F1-scores for barren, and snow and ice are errors in the SRTM, both in terms of geolocation relative to Landsat and the SRTM height estimates. In high relief areas with steep slopes and high elevation,

SRTM tends to underestimate both slope and elevation (Guth, 2006; Mukul et al., 2017), and that may have adversely affected our topographic corrections. The highest disagreement rate between the two classification maps occurred in areas with extreme illumination conditions. In these areas, rangeland pixels were misclassified as deciduous forest, and deciduous forest was misclassified as mixed forest, when using uncorrected imagery. This is in line with a previous study that found that land-cover mapping accuracies for uncorrected images were lowest in very low and high illuminated areas (Moreira and Valeriano, 2014). Results from Vanonckelen et al. (2013) show similar results that the largest accuracy improvements were obtained in low illuminated areas. The disagreement between our two maps was lowest in areas where cos Θ_S and cos i were similar, which is the case in areas where
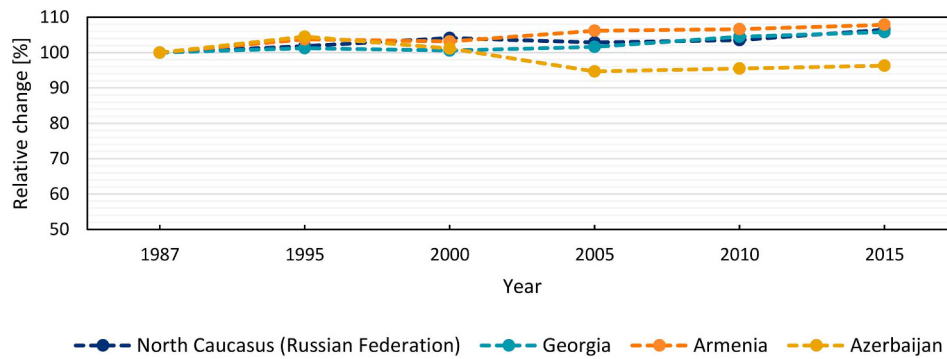
Fig. 10. Relative forest change for six time steps with 1987 as baseline for the North Caucasus (Russian Federation), Georgia, Armenia and Azerbaijan. Note that the y-axis starts at 50%.
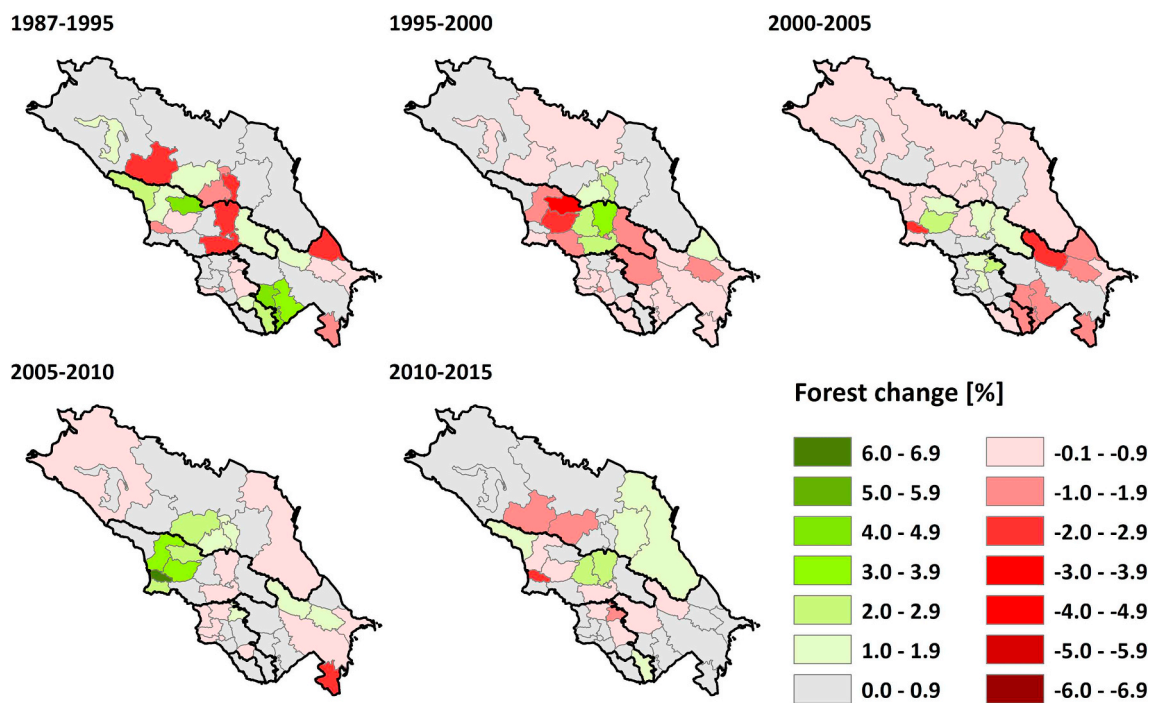

Fig. 11. Forest change aggregated for administrative units of the North Caucasus (Russian Federation), Georgia, Armenia and Azerbaijan. Please refer to supplemental information Fig. A10 for names of administrative units.

Table 1

Error matrix (area proportion in percent) for user's accuracy (UA) and producer's accuracy (PA) for cropland change map (NC = non-cropland, TC = transitional cropland, SC = stable cropland, CG = cropland gain, CL = cropland loss) for topographically-corrected images for the five time intervals.

		Reference													
	Class	NC	TC	SC	CG15	CG10	CG05	CG00	CG95	CL95	CL00	CL05	CL10	CL15	UA
Classification	NC	52.05	0.00	0.72	0.36	0.00	0.00	0.00	0.00	0.36	0.00	0.36	0.00	0.00	96.67
	TC	8.55	7.39	0.92	0.00	0.00	0.00	0.00	0.00	0.23	0.23	0.00	0.00	0.00	42.67
	SC	1.54	3.51	15.01	0.00	0.00	0.00	0.14	0.14	0.00	0.00	0.14	0.42	0.14	71.33
	CG15	0.61	0.08	0.00	0.07	0.05	0.00	0.00	0.00	0.02	0.00	0.02	0.00	0.00	8.00
	CG10	0.25	0.04	0.01	0.01	0.07	0.01	0.02	0.00	0.00	0.00	0.00	0.00	0.00	18.00
	CG05	0.17	0.05	0.01	0.00	0.01	0.05	0.00	0.00	0.00	0.01	0.00	0.00	0.00	16.00
	CG00	0.21	0.04	0.03	0.00	0.01	0.01	0.03	0.00	0.00	0.00	0.00	0.00	0.00	10.00
	CG95	0.30	0.21	0.19	0.00	0.06	0.00	0.06	0.11	0.02	0.00	0.00	0.00	0.00	12.00
	CL95	1.60	0.13	0.00	0.00	0.00	0.00	0.00	0.00	0.43	0.00	0.00	0.00	0.00	20.00
	CL00	0.40	0.08	0.00	0.00	0.00	0.00	0.00	0.00	0.11	0.14	0.06	0.00	0.00	18.00
	CL05	0.23	0.04	0.03	0.00	0.00	0.00	0.00	0.00	0.04	0.02	0.12	0.00	0.00	26.00
	CL10	0.12	0.05	0.02	0.00	0.00	0.00	0.00	0.00	0.04	0.07	0.08	0.05	0.00	12.00
	CL15	0.39	0.22	0.11	0.00	0.00	0.00	0.00	0.00	0.02	0.09	0.02	0.09	0.15	14.00
	PA	78.36	62.43	88.07	15.52	36.33	67.60	13.99	44.59	33.91	25.98	15.48	9.31	52.16	75.7 ± 2.6

Table 2
Error matrix (area proportion in percent) for user's accuracy (UA) and producer's accuracy (PA) for forest change map (NF = non-forest, TF = transitional forest, SF = stable forest, FG = forest gain, FL = forest loss) for topographically-corrected images for the five time intervals.

	Reference													
	Class	NF	TF	SF	FG15	FG10	FG05	FG00	FG95	FL95	FL00	FL05	FL10	FL15	UA
Classification	NF	73.46	0.00	0.51	1.54	1.03	0.51	0.00	0.00	0.00	0.00	0.00	0.00	0.00	95.33
	TF	1.33	0.63	1.72	0.00	0.08	0.00	0.08	0.00	0.00	0.00	0.00	0.00	0.08	16.00
	SF	0.00	0.00	15.50	0.00	0.33	0.00	0.00	0.33	0.00	0.00	0.00	0.00	0.11	95.33
	FG15	0.14	0.00	0.08	0.16	0.04	0.01	0.02	0.00	0.00	0.00	0.00	0.00	0.00	36.00
	FG10	0.04	0.00	0.05	0.03	0.07	0.02	0.01	0.02	0.00	0.00	0.00	0.00	0.00	30.00
	FG05	0.04	0.00	0.04	0.00	0.01	0.06	0.01	0.00	0.00	0.00	0.00	0.00	0.00	34.00
	FG00	0.04	0.02	0.12	0.00	0.01	0.01	0.06	0.01	0.00	0.00	0.00	0.00	0.00	22.00
	FG95	0.06	0.04	0.31	0.01	0.00	0.02	0.00	0.15	0.00	0.00	0.00	0.00	0.00	26.00
	FL95	0.37	0.01	0.07	0.00	0.00	0.00	0.00	0.00	0.02	0.02	0.00	0.00	0.00	4.00
	FL00	0.09	0.00	0.04	0.00	0.00	0.00	0.00	0.00	0.01	0.02	0.01	0.00	0.00	12.00
	FL05	0.03	0.01	0.02	0.00	0.00	0.00	0.00	0.00	0.00	0.01	0.03	0.01	0.00	24.00
	FL10	0.03	0.00	0.03	0.00	0.00	0.00	0.00	0.00	0.00	0.00	0.00	0.02	0.01	20.00
	FL15	0.04	0.00	0.09	0.00	0.00	0.00	0.00	0.00	0.00	0.00	0.00	0.00	0.03	20.00
	PA	97.07	87.71	83.43	9.24	4.73	9.18	34.28	29.84	63.66	40.58	77.93	53.50	14.06	90.2 ± 2.7

the topographic effect is minimum, such as in flat terrain, which was in our study area especially the case in the Northern Caucasus. We further found that within the total area where the land-cover classification differed, shaded pixels were more common than brightened pixels. For brightened pixels topographic correction mainly has to correct for geometric terms, whereas in shaded areas, direct illumination is reduced, resulting in larger correction factor areas, and consequently higher disagreement rates, too. This result is in line with Dorren et al. (2003), who found that classification errors for uncorrected images are more common for pixels with high incidence angles. Another reason for the lower disagreement rates in brightened areas may be the favored distribution of training samples in sunlit areas and therefore an optimized classification result (Meyer et al., 1993).

We found that in mountainous regions topographic correction is particularly valuable for distinguishing forest types, especially in a study region such as the Caucasus, where most forest occurs in rugged terrain. The mixed forest class had the highest disagreement between the non-topographically-corrected and topographically-corrected maps, which is similar to previous studies (Hill et al., 1995; Meyer et al., 1993). When illumination conditions are high, mixed forest is misclassified as deciduous forest, and when illumination conditions are low, mixed forest is misclassified as coniferous forest. By using topographically-corrected imagery, we greatly reduced the classification error among forest types, thereby improving the F1-score for all three forest types.

4.2. Cropland and forest change assessment

Our study presents the first broad-scale land-cover change assessment for the Caucasus Mountains that spans the entire 30-m resolution Landsat record. We successfully mapped cropland and forest changes over a large spatial extent with high-temporal frequency. By mapping the Caucasus Mountains frequently and identifying the timing of cropland and forest change, we provide important information to understand determinants for land change processes.

We found a general decline in cropland from 1987 to 2000 (North Caucasus, Georgia, Armenia) and 2005 (Azerbaijan), similar to what occurred elsewhere in Eastern Europe and former Soviet Union countries (Estel et al., 2015; Kraemer et al., 2015; Kuemmerle et al., 2006; Schierhorn et al., 2013). However, we were surprised to find though that the North Caucasus had much less cropland loss than temperate European Russia, the Baltics, and Ukraine (Alcantara et al., 2013; Prishchepov et al., 2013). Our rates of cropland loss were also considerably lower than what had been previously estimated based on the mapping of early-successional woody vegetation as a proxy of abandonment, but those maps were based on 250-m MODIS data (Alcantara

et al., 2013), which may be too coarse for the finely grained cropland cover in the Caucasus Mountains (Yin et al., 2019; Yin et al., 2018b).

Interestingly, we detected much more stable cropland in the North Caucasus compared to Georgia, Armenia, and Azerbaijan, although the agricultural sector of all four countries underwent major land reforms after the collapse of the Soviet Union (Lerman, 2006). A possible explanation for observed differences may be the differences in land distribution (Spoor, 2012). In Georgia, Armenia, and Azerbaijan, land of collective farms was distributed among community members and villagers (Hartvigsen, 2014). Communities with higher population density received smaller parcels resulting in highly fragmented land ownership, which may have hampered cultivation if parcels were far apart from each other. In contrast, in the Russian Federation, land distribution was carried out through land shares and the structure of the collective farms was often maintained resulting in less ownership fragmentation (Hartvigsen, 2014; Spoor, 2012). Another possible reason for higher rates of stable agriculture in the North Caucasus could be market demand, market accessibility and cost of cultivation (Rada et al., 2017). In the North Caucasus, the internal demand and access to the main market (the Russian Federation) did not change considerably shortly after the collapse of the Soviet Union. In the South Caucasus however, crop production that was oriented towards the Russian market (e.g. tea) became problematic, due to, among others factors, increased transportation costs and rising competition with other countries (Kochlamazashvili and Kakulia, 2013; O'Loughlin et al., 2007). Further, the plains of the North Caucasus with fertile chernozem soils and good climatic conditions make cultivation much easier than the hilly terrain of the South Caucasus (Afonin et al., 2008; de Beurs et al., 2017). The South Caucasus, especially the eastern part, is also prone to climate change. Droughts, heat events and water stress, as well as insufficiently managed irrigation and drainage systems, make cropland cultivation challenging (Ahouissoussi et al., 2014; Elizbarashvili et al., 2018).

We found that forest change rates in the Caucasus between 1987 and 2015 were smaller than forest changes in Central and Eastern Europe, and the former Soviet Union during the same time (Baumann et al., 2012; Griffiths et al., 2014; Potapov et al., 2015), which also surprised us. In general, we found a slight increase in forest cover for the North Caucasus, Georgia and Armenia since 1987, but a decrease until 2005 for Azerbaijan. Forest gain was often due to the conversion of cropland or rangeland to forest. Forest recovery on abandoned agricultural fields is common across former Soviet countries (Griffiths et al., 2014). Our results generally matched those from prior case studies of parts of our study area. For the war-torn regions Chechnya and Nagorno-Karabakh, located in Kalbajar-Lachin and Yukhari-Karabakh, we found very low rates of both forest loss and forest gain, and cropland change dominated, similar to previous results (Baumann et al., 2015;

Yin et al., 2018b). For Georgia, a previous study found 0.8% forest loss from 1990 to 2000 and forest gain was miniscule (0.09%, (Olofsson et al., 2010). We found an overall slight increase of 1.17% in forest cover between 1987 and 2000 across Georgia and some forest gains along forests edges and on abandoned fields in Abkhazia, which may be related to the armed conflict there in the early 1990s. In the North Caucasus, our results are in line with a previous study that detected large areas of forest loss related to the Olympic Games in Sochi in 2014 (Bragina et al., 2015).

In general, the reasons for forest change in the Caucasus Mountains are multifold, but are most likely primarily a result of the political situation, illegal logging, and sheep and cattle grazing (FAO, 2019). The increase in forest in Georgia and Armenia is likely related to the reduction of sheep grazing. After the collapse of the Soviet Union not only did the demand for sheep decrease, but the herds from Georgia also lost access to winter pastures in Dagestan (North Caucasus) (Radvanyi and Muduyev, 2007). As a result, forests started to regrow on former pastures in the mountains. A similar decline in sheep herds was observed in Armenia, when the Azerbaijani population moved to Azerbaijan after the start of the Nagorno-Karabakh conflict and forests started to regrow in some areas of former rangelands located within forested zones. Yet, in Azerbaijan pressure from sheep grazing on mountain grasslands increased since the collapse of the Soviet Union and may have resulted in forest loss (de Leeuw et al., 2019) and cattle grazing inside forests is causing forest degradation (UNECE and FAO, 2019). Another reason for forest loss in all four countries between 1987 and 2000/2005 was the unstable political situation. The forest sectors suffered from weak law enforcement and illegal logging both for fuelwood by the local population and for wood export by companies (FAO, 2015; Ozdogan et al., 2017). Illegal forest cutting has been identified as one of the main threats to biodiversity in the Caucasus (Zazanashvili et al., 2012). However, most forests occur in high elevation making transportation costly. Further, the establishment of many protected areas with relatively high protection status in the last 20 years likely protected forest from large clear cuts and broad-scale exploitation.

4.3. Limitations

To our knowledge, this is the first broad-scale land-cover change assessment for the Caucasus Mountains back to the 1980s. However, we acknowledge that our maps have some limitations. In order to account for the climatic variability in our study region we integrated phenology for each pixel. Unfortunately, the number of cloud-free Landsat pixels was very limited in some years and consequently we had to average phenology across all years. Moreover, to generate gap-free composites we had to use satellite observations acquired within 1 or 2 years of the target year. Both steps reduced the temporal accuracy of our maps. This is why we restricted our land-cover change assessment to only two trajectories (gain and loss) and aggregated more complex changes to one transitional class, which improved change classification accuracies but prohibited an analysis of re-cultivation. Further, because of the lack of ground truth, most of our training samples were gathered using visual image interpretation. Labeling errors may have biased our accuracy assessment, but collecting a sufficient amount of error-free reference to validate land-use change maps over a large area is challenging (Stehman and Foody, 2019), and was not feasible for our study.

Our change detection maps had overall high accuracy, but user's and producer's accuracies for change classes were low. Validating a large number of change classes is challenging, especially for small change classes (Stehman and Foody, 2019). In our case, 19 out of the 20 change classes covered less than 1% of the study area, making it difficult to achieve high area adjusted user's and producer's accuracies. However, change classes often showed confusion with the previous or following time step, indicating that the changes are mapped correctly, but the exact timing may be shifted by one time step. Cropland change mapping is especially difficult in areas where the climate is highly variable, and where a variety of cropland cultivation methods are applied. Furthermore, non-intensively managed fields in arid regions are spectrally very similar to rangelands. For forest change maps, forest gain is typically more difficult to map than forest loss, because it occurs gradually and its timing is difficult to determine (Hansen et al., 2010; Li et al., 2017). Spectral similarities between orchards, vineyards, and forests also resulted in some classification errors. Lastly, we were not able to detect sub-pixel-level changes, which is unfortunate because overgrazing and selective logging are the dominant threats to forests, not large clear cuts (FAO, 2019).

5. Conclusion

We applied an integrated atmospheric and topographic correction approach and mapped land-cover changes in the Caucasus Mountains from 1987 to 2015 based on the full Landsat archive. In deriving our topographically-corrected land-cover classification, we demonstrated that it is feasible to correct for topographic effects when mapping large areas. The resulting maps were considerably more accurate, especially where the terrain is steep. It follows that we recommend making an integrated atmospheric and topographic correction of Landsat satellite imagery a matter of routine in mountainous regions to ensure accurate land-cover classifications. We found that the majority of the land-cover changes in the Caucasus were related to cropland changes that occurred between 1987 and 2005. Cropland was much more stable in the northern part of the Caucasus (the Russian Federation) compared to the southern countries, Georgia, Armenia, and Azerbaijan. In the South Caucasus, cropland was much more variable and the amount of cultivated cropland dropped especially from 2000 to 2005. Few changes occurred in forests, and forest loss and forest gain had similar magnitude. The observed changes are most likely connected to the collapse of the Soviet Union in 1991, and the subsequent land reforms and armed conflicts during the 1990s.

Data availability

All land-cover maps can be downloaded at http://silvis.forest.wisc.edu/maps-data/caucasus.

Declaration of Competing Interest

The authors declare that they have no known competing financial interests or personal relationships that could have appeared to influence the work reported in this paper.

Appendix A. Methods - FORCE and implemented topographic correction

The framework for operational radiometric correction for environmental monitoring (FORCE) is a software to enable mass-processing of medium-resolution satellite imagery for large area applications. The FORCE Level 2 Processing system (L2PS) masks clouds, cloud shadows and snow pixels

with an extended Fmask algorithm, which drops the termination criterion to increase cloud classification producer's accuracy, and includes a darkness filter to counteract false positives in dryland areas (modifications are described in Frantz et al., 2015; Zhu et al., 2015; Zhu and Woodcock, 2012). The cloud masking was evaluated in the Cloud Masking Inter-comparison Exercise (Earth ESA, 2016).

The atmospheric correction in FORCE L2PS is based on radiative transfer theory (Tanre et al., 1979) and includes integrated atmospheric and topographic correction, as well as a correction for adjacency effects to estimate Bottom-of-Atmosphere (BOA) reflectance (Frantz et al., 2016). Aerosol optical depth is estimated for each image over dark water and dense dark vegetation objects using multiple scattering. A precompiled water vapor database (Frantz et al., 2019; Frantz and Stellmes, 2018) was derived from MODIS (Gao and Kaufman, 2003) to correct for gaseous absorption (Frantz et al., 2016). The performance of the atmospheric correction implemented in FORCE was compared to other approaches (including ATCOR, LaSRC, and Sen2Cor) in the Atmospheric Correction Intercomparison eXercise (ACIX) (Doxani et al., 2018). In those comparisons, FORCE produced high quality estimates of aerosol optical thickness and surface reflectance that were similar to those from LaSRC. The second edition of ACIX will include more in the depth comparison using a much larger reference dataset (Earth ESA, 2016).

The topographic correction algorithm in FORCE L2PS is an enhanced C-correction based on the theoretical principles outlined in Kobayashi and Sanga-Ngoie (2008) and on the predecessor algorithm described in Frantz et al. (2016). The topographic correction is closely integrated with atmospheric correction featuring both empirical and physical terms.

The traditional C-correction complements the cosine correction with a factor C (Teillet et al., 1982):

$$A_\lambda = \frac{\cos \Theta_S + C_\lambda}{\cos i + C_\lambda} \qquad (5)$$

where cos i represents the illumination angle and is defined as:

$$\cos i = \cos \Theta_S \cos \Theta_n + \sin \Theta_S \sin \Theta_n \cos(\Phi_S - \Phi_n) \qquad (6)$$

with Θ_S being the solar zenith angle, Θ_n the topographic slope angle, Φ_S is the solar azimuth angle, and Φ_n is the aspect angle of the topographic surface (Civco, 1989). Cos i ranges from -1 (minimum illumination) to 1 (maximum illumination). Values below 0 do not receive direct radiance. The subscript λ indicates terms that are dependent on wavelength.

The C-factor is assumed to model the contribution of the diffuse illumination (Teillet et al., 1982) and thus the C-correction is less affected by overcorrection in poorly illuminated areas because C_λ has a moderating influence on the cosine correction (Teillet et al., 1982). Commonly, C_λ is empirically derived from a linear regression between the at-satellite radiance or reflectance and the illumination angle:

$$C_\lambda = \frac{b_\lambda}{m_\lambda} \qquad (7)$$

with b_λ and m_λ being the intercept and slope of the regression line, respectively. The empirical estimation of C_λ accounts for non-Lambertian scattering of the surface target (Teillet et al., 1982). However, due to different Lambertian characteristics of different land surfaces, it is generally advised to estimate C_λ for at least vegetated and non-vegetated surfaces separately, e.g., by applying an NDVI threshold and to exclude relatively flat pixels (e.g. Hantson and Chuvieco, 2011). Frantz et al. (2016) analyzed the performance of approx. 40,000 C-corrected Landsat images, and results indicated that the correction was generally successful for the near and shortwave infrared bands, whereas topographic correction results for the visible bands were not a substantial improvement over non-corrected imagery for a considerable share of images. Frantz et al. (2016) concluded that this was likely due to the lack of a relationship between radiance and illumination angle in the visible bands when aerosol optical depth was high, i.e., when a strong and spatially homogeneous diffuse illumination component affected both sunlit and shaded areas.

Kobayashi and Sanga-Ngoie (2008) proposed that the topographic correction factor A_λ can be expressed with consideration of diffuse and direct illumination components as:

$$A_\lambda = \frac{\cos \Theta_S + f_\lambda \cos \Theta_S}{\cos i + h f_\lambda \cos \Theta_S} \qquad (8)$$

where h is the portion of the sky dome diffusing on to the tilted surface:

$$h = \frac{1 - \Theta_n}{\pi} \; (\Theta_n \text{ in radians}) \qquad (9)$$

and f_λ is the proportionality factor between the direct $E_{b,\lambda}$ and the diffuse $E_{d,\lambda}$ irradiance reaching the horizontal surface:

$$f_\lambda = \frac{E_{d,\lambda}}{E_{b,\lambda}} \qquad (10)$$

Kobayashi and Sanga-Ngoie (2008) derived that C_λ can be expressed as:

$$C_\lambda = h_0 f_\lambda \cos \Theta_S \qquad (11)$$

with h_0 being the h-factor at cos $i = 0$, and can be expressed as:

$$h_0 = \frac{\pi + 2\Theta_S}{2\pi} \; (\Theta_S \text{ in radians}) \qquad (12)$$

When combining eq. 8 and 11, the A-factor becomes:

$$A_\lambda = \frac{\cos \Theta_S + C_\lambda h_0^{-1}}{\cos i + C_\lambda h_0^{-1} h} \qquad (13)$$

Thus, if direct and diffuse illumination terms are known, and that is the case when the topographic correction is integrated with atmospheric correction, the topographic correction factor can be computed. However, the reader may notice that this formulation of C_λ only takes into account the diffuse illumination, but not land surface characteristics such as non-Lambertian behavior. Therefore, an image-based estimation of C_λ might still be more practical. Nevertheless, as 1) C_λ can be modelled when direct and diffuse components are available, and 2) the empirical estimation of C is

most successful for the SWIR2 band, but 3) might fail for the visual bands, it is feasible to empirically estimate C in the SWIR2 band only (C_{SW2}) and then propagate through the spectrum to any other wavelength. From eq. 11, it follows that the wavelength-dependency of C_λ is only due to f_λ. Thus, C_λ can be computed from C_{SW2} as:

$$C_\lambda = C_{SW2} \, f_{SW2}^{-1} \, f_\lambda \tag{14}$$

As shown in literature, it is most desirable to estimate C_{SW2} for each land-cover class individually to capture different land surface characteristics. Our approach thus estimated C_{SW2} for each pixel individually. However, this is computationally expensive, thus, we only estimated C_{SW2} for lower illumination areas ($\cos i < \cos \Theta_S$), whereas C_{SW2} was computed with eq. 11 for sunlit areas where overcorrections were less problematic. No topographic correction was attempted for deep shadow areas ($\cos i < 0$), and we assumed that topographic correction became less reliable for $i > 80°$ (Flood et al., 2013). For relatively flat pixels (slope $< 2°$), the traditional cosine correction was used. Please see an example map of C_{SW2} in SI Fig. A11 for one Landsat image.

In order to calculate C_{SW2} for each pixel, it is necessary to include pixels from its neighborhood to parameterize the linear regression. Tan et al. (2013) suggested to use 3×3 km kernels for their empirical correction, which we basically adopted. Nevertheless, for performance considerations we only used sparse sampling, wherein the area closer to the central pixel was more densely sampled. Flat pixels (slope $< 2°$) were excluded from the linear regression. Pixels that were in a different land-cover class were excluded, too. Commonly, this is achieved using a fixed NDVI threshold of e.g., 0.4. However, this was disadvantageous in two respects: 1) this arbitrary division is ill-suited for pixels that are close to this threshold and 2) NDVI only separates vegetated a non-vegetated areas, thus e.g., forest and grassland are in the same class although they have substantially different Lambertian characteristics. Therefore, we used a (SWIR1 - SWIR2) / (SWIR1 + SWIR2) threshold, which we found more meaningful when estimating C for the SWIR band. In addition, we did not use a fixed threshold but accepted a pixel if it differs less than + / - 0.025 from the central pixel. If C could not be estimated (e.g., because there were not enough samples or negative retrieval), the computed C (eq. 11) was used instead.

Appendix B. Supplementary data

Supplementary data to this article can be found online at https://doi.org/10.1016/j.rse.2020.111967.

References

Afonin, A.N., Greene, S.L., Dzyubenko, N.I., Frolow, A.N., 2008. Interactive Agricultural Ecological Atlas of Russia and Neighboring Countries. Economic Plants and their Diseases, Pests and Weeds [Online] [WWW Document]. URL. http://www.agroatlas.ru.

Ahouissoussi, N., Neumann, J.E., Srivastava, J.P., 2014. Building resilience to climate change in South Caucasus agriculture (no. 87601). The World Bank.

Alcantara, C., Kuemmerle, T., Baumann, M., Bragina, E.V., Griffiths, P., Hostert, Patrick, Knorn, J., Müller, D., Prishchepov, A.V., Schierhorn, F., Sieber, A., Radeloff, V.C., 2013. Mapping the extent of abandoned farmland in Central and Eastern Europe using MODIS time series satellite data. Environ. Res. Lett. 8, 035035. https://doi.org/10.1088/1748-9326/8/3/035035.

Balthazar, V., Vanacker, V., Lambin, E.F., 2012. Evaluation and parameterization of ATCOR3 topographic correction method for forest cover mapping in mountain areas. Int. J. Appl. Earth Obs. Geoinf. 18, 436–450. https://doi.org/10.1016/j.jag.2012.03.010.

Baumann, M., Ozdogan, M., Kuemmerle, T., Wendland, K.J., Esipova, E., Radeloff, V.C., 2012. Using the Landsat record to detect forest-cover changes during and after the collapse of the Soviet Union in the temperate zone of European Russia. Remote Sens. Environ. 124, 174–184. https://doi.org/10.1016/j.rse.2012.05.001.

Baumann, M., Radeloff, V.C., Avedian, V., Kuemmerle, T., 2015. Land-use change in the Caucasus during and after the Nagorno-Karabakh conflict. Reg. Environ. Chang. 15, 1703–1716. https://doi.org/10.1007/s10113-014-0728-3.

Bhatta, K.P., Grytnes, J.-A., Vetaas, O.R., 2018. Downhill shift of alpine plant assemblages under contemporary climate and land-use changes. Ecosphere 9, e02084. https://doi.org/10.1002/ecs2.2084.

Bleyhl, B., Baumann, M., Griffiths, P., Heidelberg, A., Manvelyan, K., Radeloff, V.C., Zazanashvili, N., Kuemmerle, T., 2017. Assessing landscape connectivity for large mammals in the Caucasus using Landsat 8 seasonal image composites. Remote Sens. Environ. 193, 193–203. https://doi.org/10.1016/j.rse.2017.03.001.

Bragina, E.V., Radeloff, V.C., Baumann, M., Wendland, K., Kuemmerle, T., Pidgeon, A.M., 2015. Effectiveness of protected areas in the Western Caucasus before and after the transition to post-socialism. Biol. Conserv. 184, 456–464. https://doi.org/10.1016/j.biocon.2015.02.013.

Civco, D.L., 1989. Topographic normalization of Landsat thematic mapper digital imagery. Photogramm. Eng. Remote. Sens. 55, 1303–1309.

Congalton, R.G., 1991. A review of assessing the accuracy of classifications of remotely sensed data. Remote Sens. Environ. 37, 35–46. https://doi.org/10.1016/0034-4257(91)90048-B.

de Beurs, K., Ioffe, G., Nefedova, T., Henebry, G., 2017. Land change in European Russia: 1982–2011. In: Gutman, G., Radeloff, V. (Eds.), Land-Cover and Land-Use Changes in Eastern Europe after the Collapse of the Soviet Union in 1991. Springer International Publishing, Cham, pp. 223–241. https://doi.org/10.1007/978-3-319-42638-9_10.

de Leeuw, J., Rizayeva, A., Namazov, E., Bayramov, E., Marshall, M.T., Etzold, J., Neudert, R., 2019. Application of the MODIS MOD 17 net primary production product in grassland carrying capacity assessment. Int. J. Appl. Earth Obs. Geoinf. 78, 66–76. https://doi.org/10.1016/j.jag.2018.09.014.

Dorren, L.K.A., Maier, B., Seijmonsbergen, A.C., 2003. Improved Landsat-based forest mapping in steep mountainous terrain using object-based classification. For. Ecol. Manag. 183, 31–46. https://doi.org/10.1016/S0378-1127(03)00113-0.

Doxani, G., Vermote, E., Roger, J.-C., Gascon, F., Adriaensen, S., Frantz, D., Hagolle, O., Hollstein, A., Kirches, G., Li, F., Louis, J., Mangin, A., Pahlevan, N., Pflug, B., Vanhellemont, Q., 2018. Atmospheric correction inter-comparison exercise. Remote Sens. 10, 352. https://doi.org/10.3390/rs10020352.

Earth ESA, 2016. ACIX II - CMIX 1st WS [WWW Document]. URL. https://earth.esa.int/web/sppa/meetings-workshops/hosted-and-co-sponsored-meetings/acix-ii-cmix (accessed 6.2.20).

EEA, 2010. Europe's Ecological Backbone: Recognising the True Value of our Mountains. European Environment Agency EEA, Copenhagen.

Elizbarashvili, N., Meessen, H., Khoetsyan, A., Meladze, G., Kohler, T., 2018. Sustainable development of mountain regions and resource management. Publish House "DANI," Tbilisi.

Estel, S., Kuemmerle, T., Alcántara, C., Levers, C., Prishchepov, A., Hostert, P., 2015. Mapping farmland abandonment and recultivation across Europe using MODIS NDVI time series. Remote Sens. Environ. 163, 312–325. https://doi.org/10.1016/j.rse.2015.03.028.

FAO, 2015. Global Forest Resources Assessment 2015. How Are the world's Forests Changing? Food and Agriculture Organization of the United Nations, Rome, Italy.

FAO, 2019. State of Forests of the Caucasus and Central Asia. Food and Agriculture Organization of the United Nations, New York and Geneva.

Flood, N., Danaher, T., Gill, T., Gillingham, S., 2013. An operational scheme for deriving standardised surface reflectance from Landsat TM/ETM+ and SPOT HRG Imagery for Eastern Australia. Remote Sens. 5, 83–109. https://doi.org/10.3390/rs5010083.

Frantz, D., 2019. FORCE—Landsat + Sentinel-2 analysis ready data and beyond. Remote Sens. 11, 1124. https://doi.org/10.3390/rs11091124.

Frantz, D., Stellmes, M., 2018. Water vapor database for atmospheric correction of Landsat imagery. Suppl. Frantz David Röder Achim Stellmes Marion Hill Joachim 2016 Oper. Radiom. Landsat preprocessing Framew. Large-Area Time Ser. Appl. IEEE Trans. Geosci. Remote Sens. 547, 3928–3943. https://doi.org/10.1594/PANGAEA.893109.

Frantz, D., Röder, A., Udelhoven, T., Schmidt, M., 2015. Enhancing the detectability of clouds and their shadows in multitemporal dryland Landsat imagery: extending Fmask. IEEE Geosci. Remote Sens. Lett. 12, 1242–1246. https://doi.org/10.1109/LGRS.2015.2390673.

Frantz, D., Röder, A., Stellmes, M., Hill, J., 2016. An operational radiometric Landsat preprocessing framework for large-area time series applications. IEEE Trans. Geosci. Remote Sens. 54, 4153–4164. https://doi.org/10.1109/TGRS.2016.2530856.

Frantz, D., Röder, A., Stellmes, M., Hill, J., 2017. Phenology-adaptive pixel-based compositing using optical earth observation imagery. Remote Sens. Environ. 190, 331–347. https://doi.org/10.1016/j.rse.2017.01.002.

Frantz, D., Stellmes, M., Hostert, P., 2019. A global MODIS water vapor database for the operational atmospheric correction of historic and recent Landsat imagery. Remote Sens. 11, 257. https://doi.org/10.3390/rs11030257.

Friedl, M.A., McIver, D.K., Hodges, J.C.F., Zhang, X.Y., Muchoney, D., Strahler, A.H., Woodcock, C.E., Gopal, S., Schneider, A., Cooper, A., Baccini, A., Gao, F., Schaaf, C., 2002. Global land cover mapping from MODIS: algorithms and early results. Remote Sens. Environ., The Moderate Resolution Imaging spectroradiometer (MODIS): a new generation of Land Surface Monitoring 83, 287–302. https://doi.org/10.1016/S0034-4257(02)00078-0.

Gao, B.-C., Kaufman, Y.J., 2003. Water vapor retrievals using moderate resolution imaging spectroradiometer (MODIS) near-infrared channels. J. Geophys. Res.-Atmos. 108, 4389. https://doi.org/10.1029/2002JD003023.

García-Ruiz, J.M., Lasanta, T., Ruiz-Flano, P., Ortigosa, L., White, S., González, C., Martí, C., 1996. Land-use changes and sustainable development in mountain areas: a case study in the Spanish Pyrenees. Landsc. Ecol. 11, 267–277. https://doi.org/10.1007/BF02059854.

Gellrich, M., Zimmermann, N.E., 2007. Investigating the regional-scale pattern of agricultural land abandonment in the Swiss mountains: a spatial statistical modelling approach. Landsc. Urban Plan. 79, 65–76. https://doi.org/10.1016/j.landurbplan.2006.03.004.

Giovarelli, R., Bledsoe, D., 2001. Land Reform in Eastern Europe, Western CIS, Transcaucasus, Balkans, and EU Accession Countries. Seattle, Washington.

Gómez, C., White, J.C., Wulder, M.A., 2016. Optical remotely sensed time series data for land cover classification: a review. ISPRS J. Photogramm. Remote Sens. 116, 55–72. https://doi.org/10.1016/j.isprsjprs.2016.03.008.

Gorelick, N., Hancher, M., Dixon, M., Ilyushchenko, S., Thau, D., Moore, R., 2017. Google Earth engine: planetary-scale geospatial analysis for everyone. Remote Sens. Environ. Big Remotely Sensed Data: tools, applications and experiences 202, 18–27. https://doi.org/10.1016/j.rse.2017.06.031.

Griffiths, P., van der Linden, S., Kuemmerle, T., Hostert, P., 2013. A pixel-based Landsat compositing algorithm for large area land cover mapping. IEEE J. Sel. Top. Appl. Earth Obs. Remote Sens. 6, 2088–2101. https://doi.org/10.1109/JSTARS.2012.2228167.

Griffiths, P., Kuemmerle, T., Baumann, M., Radeloff, V.C., Abrudan, I.V., Lieskovsky, J., Munteanu, C., Ostapowicz, K., Hostert, P., 2014. Forest disturbances, forest recovery, and changes in forest types across the Carpathian ecoregion from 1985 to 2010 based on Landsat image composites. Remote Sens. Environ., special issue on 2012 ForestSAT 151, 72–88. https://doi.org/10.1016/j.rse.2013.04.022.

Gulisashvili, V.Z., 1964. Prirodnye Zony I Estestvenno-Istoricheskie Oblasti Kavkaza (Natural Zones and Historical Environmental Regions in the Caucasus). Nauka Publ, Mosc 327 pp.

Guth, P.L., 2006. Geomorphometry from SRTM: comparison to NED. Photogramm. Eng. Remote. Sens. 72, 269–277.

Hansen, M.C., Stehman, S.V., Potapov, P.V., 2010. Quantification of global gross forest cover loss. Proc. Natl. Acad. Sci. U. S. A. 107, 8650–8655. https://doi.org/10.1073/pnas.0912668107.

Hantson, S., Chuvieco, E., 2011. Evaluation of different topographic correction methods for Landsat imagery. Int. J. Appl. Earth Obs. Geoinf. 13, 691–700. https://doi.org/10.1016/j.jag.2011.05.001.

Hartvigsen, M.B., 2013. Land Reform in Central and Eastern Europe after 1989 and its outcome in form of farm structures and land fragmentation (FAO Land Tenure Working No. 24).

Hartvigsen, M., 2014. Land reform and land fragmentation in central and Eastern Europe. Land Use Policy 36, 330–341. https://doi.org/10.1016/j.landusepol.2013.08.016.

Hill, J., Mehl, W., Radeloff, V., 1995. Improved forest mapping by combining corrections of atmospheric and topographic effects in Landsat TM imagery. In: Askne, J. (Ed.), Sensors and Environmental Applications of Remote Sensing. Balkena, Rotterdam, pp. 143–151.

Holland, E.C., 2016. Economic development and subsidies in the North Caucasus. Probl. Post-Communism 63, 50–61. https://doi.org/10.1080/10758216.2015.1067750.

Huang, H., Gong, P., Clinton, N., Hui, F., 2008. Reduction of atmospheric and topographic effect on Landsat TM data for forest classification. Int. J. Remote Sens. 29, 5623–5642. https://doi.org/10.1080/01431160802082148.

Huntington, J.L., Hegewisch, K.C., Daudert, B., Morton, C.G., Abatzoglou, J.T., McEvoy, D.J., Erickson, T., 2017. Climate engine: cloud computing and visualization of climate and remote sensing data for advanced natural resource monitoring and process understanding. Bull. Am. Meteorol. Soc. 98, 2397–2410. https://doi.org/10.1175/BAMS-D-15-00324.1.

Kobayashi, S., Sanga-Ngoie, K., 2008. The integrated radiometric correction of optical remote sensing imageries. Int. J. Remote Sens. 29, 5957–5985. https://doi.org/10.1080/01431160701881889.

Kochlamazashvili, I., Kakulia, N., 2013. The Georgian Tea Sector: A Value Chain Study. ENPARD - European Neighbourhood Programme for Agriculture and Rural Development, Tbilisi, Georgia.

Kraemer, R., Prishchepov, A.V., Müller, D., Kuemmerle, T., Radeloff, V.C., Dara, A., Terekhov, A., Frühauf, M., 2015. Long-term agricultural land-cover change and potential for cropland expansion in the former Virgin Lands area of Kazakhstan. Environ. Res. Lett. 10, 054012. https://doi.org/10.1088/1748-9326/10/5/054012.

Kuemmerle, T., Radeloff, V.C., Perzanowski, K., Hostert, P., 2006. Cross-border comparison of land cover and landscape pattern in Eastern Europe using a hybrid classification technique. Remote Sens. Environ. 103, 449–464. https://doi.org/10.1016/j.rse.2006.04.015.

Kuemmerle, T., Chaskovskyy, O., Knorn, J., Radeloff, V.C., Kruhlov, I., Keeton, W.S., Hostert, P., 2009. Forest cover change and illegal logging in the Ukrainian Carpathians in the transition period from 1988 to 2007. Remote Sens. Environ. 113, 1194–1207. https://doi.org/10.1016/j.rse.2009.02.006.

Kuhn, M., Quinlan, R., 2018. C50: C5.0 Decision Trees and Rule-Based Models. R package version 0.1.2.

Kulakowski, D., Bebi, P., Rixen, C., 2011. The interacting effects of land use change, climate change and suppression of natural disturbances on landscape forest structure in the Swiss Alps. Oikos 120, 216–225. https://doi.org/10.1111/j.1600-0706.2010.18726.x.

Lerman, Z., 2006. The impact of land reform on rural household incomes in Transcaucasia. Eurasian Geogr. Econ. 47, 112–123. https://doi.org/10.2747/1538-7216.47.1.112.

Lerman, Z., 2009. Land reform, farm structure, and agricultural performance in CIS countries. China Econ. Rev., Special Issue: Agriculture in TransitionAgriculture in Transition 20, 316–326. https://doi.org/10.1016/j.chieco.2008.10.007.

Li, A., Wang, Q., Bian, J., Lei, G., Li, A., Wang, Q., Bian, J., Lei, G., 2015. An improved physics-based model for topographic correction of Landsat TM images. Remote Sens. 7, 6296–6319. https://doi.org/10.3390/rs70506296.

Li, Y., Sulla-Menashe, D., Motesharrei, S., Song, X.-P., Kalnay, E., Ying, Q., Li, S., Ma, Z., 2017. Inconsistent estimates of forest cover change in China between 2000 and 2013 from multiple datasets: differences in parameters, spatial resolution, and definitions. Sci. Rep. 7, 8748. https://doi.org/10.1038/s41598-017-07732-5.

Liang, S., 2005. Topographic correction methods. In: Kong, J.A. (Ed.), Quantitative Remote Sensing of Land Surfaces. John Wiley & Sons, Ltd, pp. 231–245. https://doi.org/10.1002/047172372X.ch7.

Lipper, L., Thornton, P., Campbell, B.M., Baedeker, T., Braimoh, A., Bwalya, M., Caron, P., Cattaneo, A., Garrity, D., Henry, K., Hottle, R., Jackson, L., Jarvis, A., Kossam, F., Mann, W., McCarthy, N., Meybeck, A., Neufeldt, H., Remington, T., Sen, P.T., Sessa, R., Shula, R., Tibu, A., Torquebiau, E.F., 2014. Climate-smart agriculture for food security. Nat. Clim. Chang. 4, 1068–1072. https://doi.org/10.1038/nclimate2437.

MacDonald, D., Crabtree, J.R., Wiesinger, G., Dax, T., Stamou, N., Fleury, P., Gutierrez Lazpita, J., Gibon, A., 2000. Agricultural abandonment in mountain areas of Europe: environmental consequences and policy response. J. Environ. Manag. 59, 47–69. https://doi.org/10.1006/jema.1999.0335.

Mader, S., 2012. A Framework for the phenological Analysis of hypertemporal Remote Sensing Data Based on Polynomial Spline Models [WWW Document]. URL. http://ubt.opus.hbz-nrw.de/volltexte/2012/783/ (accessed 9.13.16).

Meyer, P., Itten, K.I., Kellenberger, T., Sandmeier, S., Sandmeier, R., 1993. Radiometric corrections of topographically induced effects on Landsat TM data in an alpine environment. ISPRS J. Photogramm. Remote Sens. 48, 17–28. https://doi.org/10.1016/0924-2716(93)90028-L.

Moreira, E.P., Valeriano, M.M., 2014. Application and evaluation of topographic correction methods to improve land cover mapping using object-based classification. Int. J. Appl. Earth Obs. Geoinf. 32, 208–217. https://doi.org/10.1016/j.jag.2014.04.006.

Mukul, Manas, Srivastava, V., Jade, S., Mukul, Malay, 2017. Uncertainties in the shuttle radar topography Mission (SRTM) heights: insights from the Indian Himalaya and Peninsula. Sci. Rep. 7. https://doi.org/10.1038/srep41672.

Oliver, T.H., Morecroft, M.D., 2014. Interactions between climate change and land use change on biodiversity: attribution problems, risks, and opportunities. Wiley Interdiscip. Rev. Clim. Chang. 5, 317–335. https://doi.org/10.1002/wcc.271.

Olofsson, P., Torchinava, P., Woodcock, C.E., Baccini, A., Houghton, R.A., Ozdogan, M., Zhao, F., Yang, X., 2010. Implications of land use change on the national terrestrial carbon budget of Georgia. Carbon Balance Manag. 5, 4. https://doi.org/10.1186/1750-0680-5-4.

Olofsson, P., Foody, G.M., Herold, M., Stehman, S.V., Woodcock, C.E., Wulder, M.A., 2014. Good practices for estimating area and assessing accuracy of land change. Remote Sens. Environ. 148, 42–57. https://doi.org/10.1016/j.rse.2014.02.015.

O'Loughlin, J., Kolossov, V., Radvanyi, J., 2007. The Caucasus in a time of conflict, demographic transition, and economic change. Eurasian Geogr. Econ. 48, 135–156. https://doi.org/10.2747/1538-7216.48.2.135.

Ozdogan, M., Olofsson, P., Woodcock, C.E., Baccini, A., 2017. Forest changes and carbon budgets in the Black Sea region. In: Gutman, G., Radeloff, V. (Eds.), Land-Cover and Land-Use Changes in Eastern Europe after the Collapse of the Soviet Union in 1991. Springer International Publishing, Cham, pp. 149–171. https://doi.org/10.1007/978-3-319-42638-9_7.

Pimple, U., Sitthi, A., Simonetti, D., Pungkul, S., Leadprathom, K., Chidthaisong, A., 2017. Topographic correction of Landsat TM-5 and Landsat OLI-8 imagery to improve the performance of Forest classification in the mountainous terrain of Northeast Thailand. Sustainability 9, 258. https://doi.org/10.3390/su9020258.

Potapov, P.V., Turubanova, S.A., Tyukavina, A., Krylov, A.M., McCarty, J.L., Radeloff, V.C., Hansen, M.C., 2015. Eastern Europe's forest cover dynamics from 1985 to 2012 quantified from the full Landsat archive. Remote Sens. Environ. 159, 28–43. https://doi.org/10.1016/j.rse.2014.11.027.

Powers, D.M., 2011. Evaluation: from precision, recall and F-measure to ROC, informedness, markedness and correlation. J. Mach. Learn. Technol. 2, 37–63.

Prishchepov, A.V., Mueller, D., Dubinin, M., Baumann, M., Radeloff, V.C., 2013. Determinants of agricultural land abandonment in post-Soviet European Russia. Land Use Policy 30, 873–884. https://doi.org/10.1016/j.landusepol.2012.06.011.

Quinlan, J.R., 1986. Induction of decision trees. Mach. Learn. 1, 81–106. https://doi.org/10.1007/BF00116251.

Rada, N., Liefert, W., Liefert, O., 2017. Productivity Growth and the Revival of Russian agriculture (Economic Research Service No. ERR-228). U.S. Department of Agriculture.

Radvanyi, J., Muduyev, S.S., 2007. Challenges facing the mountain peoples of the Caucasus. Eurasian Geogr. Econ. 48, 157–177. https://doi.org/10.2747/1538-7216.48.2.157.

Riano, D., Chuvieco, E., Salas, J., Aguado, I., 2003. Assessment of different topographic corrections in Landsat-TM data for mapping vegetation types (2003). IEEE Trans. Geosci. Remote Sens. 41, 1056–1061. https://doi.org/10.1109/TGRS.2003.811693.

Richter, R., Kellenberger, T., Kaufmann, H., 2009. Comparison of topographic correction methods. Remote Sens. 1, 184–196. https://doi.org/10.3390/rs1030184.

Rosstat, 2010. Federal State Statistic Service, Rosstat [WWW Document]. URL. https://www.gks.ru/ (accessed 12.20.19).

Rufin, P., Frantz, D., Ernst, S., Rabe, A., Griffiths, P., Özdoğan, M., Hostert, P., 2019. Mapping cropping practices on a national scale using intra-annual Landsat time series binning. Remote Sens. 11, 232. https://doi.org/10.3390/rs11030232.

Schierhorn, F., Müller, D., Beringer, T., Prishchepov, A.V., Kuemmerle, T., Balmann, A., 2013. Post-Soviet cropland abandonment and carbon sequestration in European Russia, Ukraine, and Belarus. Glob. Biogeochem. Cycles 27, 1175–1185. https://doi.org/10.1002/2013GB004654.

Sola, I., González-Audícana, M., Álvarez-Mozos, J., 2016. Multi-criteria evaluation of

topographic correction methods. Remote Sens. Environ. 184, 247–262. https://doi. org/10.1016/j.rse.2016.07.002.

Spoor, M., 2004. Land Reform, Rural Poverty and Inequality: A pro-Poor Approach to Land Policies (UNDP Armenia White Paper). The Hague/Yerevan.

Spoor, M., 2012. Agrarian reform and transition: what can we learn from 'the east'? J. Peasant Stud. 39, 175–194. https://doi.org/10.1080/03066150.2011.652949.

Stehman, S.V., 2014. Estimating area and map accuracy for stratified random sampling when the strata are different from the map classes. Int. J. Remote Sens. 35, 4923–4939. https://doi.org/10.1080/01431161.2014.930207.

Stehman, S.V., Foody, G.M., 2019. Key issues in rigorous accuracy assessment of land cover products. Remote Sens. Environ. 231, 111199. https://doi.org/10.1016/j.rse. 2019.05.018.

Stehman, S.V., Wickham, J.D., Smith, J.H., Yang, L., 2003. Thematic accuracy of the 1992 National Land-Cover Data for the eastern United States: statistical methodology and regional results. Remote Sens. Environ. 86, 500–516. https://doi.org/10.1016/ S0034-4257(03)00128-7.

Tan, B., Masek, J.G., Wolfe, R., Gao, F., Huang, C., Vermote, E.F., Sexton, J.O., Ederer, G., 2013. Improved forest change detection with terrain illumination corrected Landsat images. Remote Sens. Environ. 136, 469–483. https://doi.org/10.1016/j.rse.2013. 05.013.

Tanre, D., Herman, M., Deschamps, P.Y., de Leffe, A., 1979. Atmospheric modeling for space measurements of ground reflectances, including bidirectional properties. Appl. Opt. 18, 3587. https://doi.org/10.1364/AO.18.003587.

Teillet, P.M., Guindon, B., Goodenough, D.G., 1982. On the slope-aspect correction of multispectral scanner data. Can. J. Remote. Sens. 8, 84–106. https://doi.org/10. 1080/07038992.1982.10855028.

Terra Institute, 2005. Final Report - Georgia Land Market Development Project. Terra Institute LTD for USAID.

UNECE, FAO, 2019. Forest Landscape Restoration in the Caucasus and Central Asia (GENEVA TIMBER AND FOREST DISCUSSION PAPER 72 No. ECE/TIM/DP/72). Switzerland, Geneva.

Vanonckelen, S., Lhermitte, S., Van Rompaey, A., 2013. The effect of atmospheric and topographic correction methods on land cover classification accuracy. Int. J. Appl. Earth Obs. Geoinf. 24, 9–21. https://doi.org/10.1016/j.jag.2013.02.003.

Vanonckelen, S., Lhermitte, S., Balthazar, V., Rompaey, A.V., 2014. Performance of atmospheric and topographic correction methods on Landsat imagery in mountain areas. Int. J. Remote Sens. 35, 4952–4972. https://doi.org/10.1080/01431161.2014. 933280.

Volodicheva, N., 2002. The Caucasus. In: Shahgedanova, M. (Ed.), The Physical Geography of Northern Eurasia. Oxford University Press, Oxford, New York, pp. 350–376.

Welton, G., Asatryan, A.A., Jijelava, D., 2013. Comparative Analysis of Agriculture in the South Caucasus. UNDP Georgia, Tbilisi, Georgia.

White, J.C., Wulder, M.A., Hobart, G.W., Luther, J.E., Hermosilla, T., Griffiths, P., Coops, N.C., Hall, R.J., Hostert, P., Dyk, A., Guindon, L., 2014. Pixel-based image compositing for large-area dense time series applications and science. Can. J. Remote. Sens. 40, 192–212. https://doi.org/10.1080/07038992.2014.945827.

Woodcock, C.E., Allen, R., Anderson, M., Belward, A., Bindschadler, R., Cohen, W., Gao, F., Goward, S.N., Helder, D., Helmer, E., Nemani, R., Oreopoulos, L., Schott, J., Thenkabail, P.S., Vermote, E.F., Vogelmann, J., Wulder, M.A., Wynne, R., 2008. Free access to Landsat imagery. Science 320, 1011. https://doi.org/10.1126/science.320. 5879.1011a.

World Bank Data, 2019a. Country Data [WWW Document]. World Bank Data, URL. https://data.worldbank.org/ (accessed 11.27.19).

World Bank Data, 2019b. Employment in Agriculture (% of Total Employment) (Modeled ILO Estimate) | Data [WWW Document]. World Bank Data. URL. https://data. worldbank.org/indicator/sl.agr.empl.zs?end=2018&start=2018&view=map (accessed 5.24.19).

Wulder, M.A., Masek, J.G., Cohen, W.B., Loveland, T.R., Woodcock, C.E., 2012. Opening the archive: how free data has enabled the science and monitoring promise of Landsat. Remote Sens. Environ., Landsat Legacy Special Issue 122, 2–10. https://doi. org/10.1016/j.rse.2012.01.010.

Yin, H., Khamzina, A., Pflugmacher, D., Martius, C., 2017. Forest cover mapping in post-soviet Central Asia using multi-resolution remote sensing imagery. Sci. Rep. 7, 1375. https://doi.org/10.1038/s41598-017-01582-x.

Yin, H., Pflugmacher, D., Li, A., Li, Z., Hostert, P., 2018a. Land use and land cover change in Inner Mongolia - understanding the effects of China's re-vegetation programs. Remote Sens. Environ. 204, 918–930. https://doi.org/10.1016/j.rse.2017.08.030.

Yin, H., Prishchepov, A.V., Kuemmerle, T., Bleyhl, B., Buchner, J., Radeloff, V.C., 2018b. Mapping agricultural land abandonment from spatial and temporal segmentation of Landsat time series. Remote Sens. Environ. 210, 12–24. https://doi.org/10.1016/j. rse.2018.02.050.

Yin, H., Butsic, V., Buchner, J., Kuemmerle, T., Prishchepov, A.V., Baumann, M., Bragina, E.V., Sayadyan, H., Radeloff, V.C., 2019. Agricultural abandonment and re-cultivation during and after the Chechen wars in the northern Caucasus. Glob. Environ. Chang. 55, 149–159. https://doi.org/10.1016/j.gloenvcha.2019.01.005.

Yin, H., Brandão, A., Buchner, J., Helmers, D., Iuliano, B.G., Kimambo, N.E., Lewińska, K.E., Razenkova, E., Rizayeva, A., Rogova, N., Spawn, S.A., Xie, Y., Radeloff, V.C., 2020a. Monitoring cropland abandonment with Landsat time series. Remote Sens. Environ. 246, 111873. https://doi.org/10.1016/j.rse.2020.111873.

Yin H., Tan B., Frantz D., Radeloff C.V., The value of topographic correction for forest classification using Landsat imagery, Remote Sens. Environ. Under review.

Zazanashvili, N., Gagnidze, R., Nakhutsrishvili, G., 1999. Main types of vegetation zonation on the mountains of the Caucasus. Acta Phytogeogr. Suec. 85, 7–16.

Zazanashvili, N., Garforth, M., Jungius, H., Gamkrelidze, T., 2012. Ecoregion Conservation Plan for the Caucasus. 2012 Revised and updated edition. Ga. Tbilisi WWF KfW BMZ.

Zhu, Z., Woodcock, C.E., 2012. Object-based cloud and cloud shadow detection in Landsat imagery. Remote Sens. Environ. 118, 83–94. https://doi.org/10.1016/j.rse. 2011.10.028.

Zhu, Z., Wang, S., Woodcock, C.E., 2015. Improvement and expansion of the Fmask algorithm: cloud, cloud shadow, and snow detection for Landsats 4–7, 8, and sentinel 2 images. Remote Sens. Environ. 159, 269–277. https://doi.org/10.1016/j.rse.2014. 12.014.